Department of Engineering Physics and Mathematics
Helsinki University of Technology
Espoo, Finland

NUMERICAL SIMULATION OF NEOCLASSICAL CURRENTS, PARALLEL VISCOSITY, AND RADIAL CURRENT BALANCE IN TOKAMAK PLASMAS

Timo Kiviniemi

Dissertation for the degree of Doctor of Science in Technology to be presented with due permission for public examination and debate in Auditorium F1 at Helsinki University of Technology (Espoo, Finland) on the 10th of August, 2001, at 12 o'clock noon.

Espoo 2001

Distribution:
Helsinki University of Technology
Department of Engineering Physics and Mathematics
Advanced Energy Systems
P.O. Box 2200
FIN-02015 HUT
FINLAND
Tel. +358-9-451 3198
Fax. +358-9-451 3195

ISBN 951-22-5537-5
ISSN 1456-3320

Otamedia Oy
Espoo 2001

Abstract

One of the principal problems en route to a fusion reactor is that of insufficient plasma confinement, which has lead to both theoretical and experimental research into transport processes in the parameter range relevant for fusion energy production. The neoclassical theory of tokamak transport is well-established unlike the theory of turbulence driven anomalous transport in which extensive progress has been made during last few years. So far, anomalous transport has been dominant in experiments, but transport may be reduced to the neoclassical level in advanced tokamak scenarios.

This thesis reports a numerical study of neoclassical fluxes, parallel viscosity, and neoclassical radial current balance in tokamaks. Neoclassical parallel viscosity and particle fluxes are simulated over a wide range of collisionalities, using the fully kinetic five-dimensional neoclassical orbit-following Monte Carlo code ASCOT. The qualitative behavior of parallel viscosity derived in earlier analytic models is shown to be incorrect for high poloidal Mach numbers. This is because the poloidal dependence of density was neglected. However, in high Mach number regime, it is the convection and compression terms, rather than the parallel viscosity term, that are shown to dominate the momentum balance. For fluxes, a reasonable agreement between numerical and analytical results is found in the collisional parameter regime. Neoclassical particle fluxes are additionally studied in the banana regime using the three-dimensional Fokker-Planck code DEPORA, which solves the drift-kinetic equation with finite differencing. Limitations of the small inverse aspect ratio approximation adopted in the analytic theory are addressed.

Assuming that the anomalous transport is ambipolar, the radial electric field and its shear at the tokamak plasma edge can be solved from the neoclassical radial current balance. This is performed both for JET and ASDEX Upgrade tokamaks using the ASCOT code. It is shown that shear high enough for turbulence suppression can be driven at the Low (L) to High (H) transition conditions without taking into account anomalous processes. In agreement with experiments, simulations indicate a higher threshold temperature for the L–H transition in JET than in ASDEX Upgrade. The parametric dependence of the shear on temperature, density, and magnetic field, however, is similar for both devices. In agreement with some theoretical models and experimental observations, the results also suggest that the critical shear for strong turbulence suppression in JET should be lower than in ASDEX Upgrade.

Preface

This work has been carried out in the Laboratory of Advanced Energy Systems at the Department of Engineering Physics and Mathematics of Helsinki University of Technology, from 1996 to 2000. The work has been carried out under the Association Euratom-TEKES Agreement.

I would like to thank my instructor Dr. Jukka Heikkinen for his guidance during the work, and for the critical reading of the manuscript. I would also like to thank all the staff of IPP Garching and JET who have helped me with this work. Especially, I am grateful to Dr. Arthur Peeters for his guidance during my three visits to Germany, Prof. Hartmut Zohm for the original suggestion to use the ASCOT code for investigating the L–H transition in ASDEX Upgrade, Prof. Kaufmann for allowing me to work at ASDEX Upgrade, and Dr. Parail for his guidance during my visit at JET. I am indebted to Dr. Seppo Sipilä for providing me with the ASCOT code and helping me with it, and to Dr. Taina Kurki–Suonio who provided me with valuable help on getting started with the orbit loss problem and, also, carefully read the manuscript. My supervisor Prof. Rainer Salomaa deserves thanks for making this work possible. All the help and guidance from my colleagues and personnel at Helsinki University of Technology and VTT Chemical Technology is gratefully acknowledged. My parents and friends are thanked for their support.

Espoo, July 23, 2001

Timo Kiviniemi

List of Publications

This paper is an introduction to the following publications:

1. T.P. Kiviniemi and J.A. Heikkinen, "Choice of constants of motion coordinates in numerical solving of the three-dimensional Fokker–Planck equation for tokamaks", Computer Physics Communications **107** (1997) pp. 149–154.

2. T.P. Kiviniemi, J.A. Heikkinen, A.G. Peeters, "Test particle simulation of nonambipolar ion diffusion in tokamaks", Nuclear Fusion **40** (2000) pp. 1587–1596.

3. T.P. Kiviniemi, J.A. Heikkinen, A.G. Peeters, "Effect of poloidal density variation on parallel viscosity for large Mach numbers", Physics of Plasmas **7** (2000) pp. 5255–5258.

4. J.A. Heikkinen, T.P. Kiviniemi, A.G. Peeters, T. Kurki-Suonio, S.K. Sipilä, W. Herrmann, W. Suttrop, H. Zohm, "Ion orbit loss current in ASDEX Upgrade", Plasma Physics and Controlled Fusion **40** (1998) pp. 693–696.

5. J.A. Heikkinen, T.P. Kiviniemi, A.G. Peeters, "Neoclassical radial current balance in tokamaks and transition to the H-mode", Physical Review Letters **84** (2000) pp. 487–490.

6. T.P. Kiviniemi, J.A. Heikkinen, A.G. Peeters, S.K. Sipilä, "Monte Carlo guiding-centre simulations of ExB flow shear in edge transport barrier", accepted for publication in Plasma Physics and Controlled Fusion.

7. T.P. Kiviniemi, T. Kurki-Suonio, S.K. Sipilä, J.A. Heikkinen, A.G. Peeters, "L-H transport barrier formation: self-consistent simulation and comparison with ASDEX Upgrade experiments", Czechoslovak Journal of Physics **49**, No. 12, Supplement S3, (1999) pp. 81–92.

Publication 1 discusses the proper choice of coordinates when solving three-dimensional neoclassical kinetic equation for low collisionality plasmas in a tokamak. Particle fluxes as a response to finite density and temperature gradients are investigated, and limitations of the large aspect ratio approximation made in analytic theory are addressed.

Publications 2-3 present Monte Carlo simulations of neoclassical particle flux and bulk viscosity in the plateau and Pfirsch-Schlüter regimes over a wide range of Mach numbers. In Publication 2, a reasonable agreement between the numerical and analytic result is found for the fluxes. The qualitative behavior of bulk viscosity is shown to be incorrect in earlier analytic calculations for high poloidal Mach number. Also, in this regime, the the convection and compression terms are shown to dominate the time behavior of parallel rotation. In Publication 3, the bulk viscosity as a function of Mach numbers is studied in more detail and the importance of the poloidal dependence of the density is addressed.

Publication 4 presents a Monte Carlo simulation of ion orbit loss current. The results are compared to the analytic expression of the neoclassical return current within the bifurcation model by Shaing. No multi-valued solutions to the current as a function of radial electric field are found in the parameter regime where L–H transition occurs in ASDEX Upgrade.

In Publications 5-7, the neoclassical current balance is investigated self-consistently without the limitations of earlier analytic approaches and of the method in Publication 4. Publication 5 confirms the result that the neoclassical current balance at the edge does not lead to bifurcating solutions although the experimental L–H transition parameters are used in the simulation. However, the shear in rotation is found to be high enough for significant turbulence suppression. The parameter scaling of the critical temperature for transition from the simulations agrees with the experimental scaling, thus suggesting that anomalous effects are not needed to explain high shear at ASDEX Upgrade L–H transition conditions. In Publication 6, the same simulation is repeated for JET and the results are compared to the ASDEX Upgrade results. The results indicate a lower critical shear for JET than for ASDEX Upgrade. The parameter dependence of the shear in rotation is investigated in more detail. In Publication 7, a numerical method to iterate the radial electric field is presented.

The disputant has actively participated in all work reported in this thesis. He was the principal author of Publications 1-3, 6 and 7. He has invented the coordinate system and written the code used in Publication 1. For Publications 2–7, he has actively participated in developing the subroutines to simulate the parallel viscosity, particle fluxes, and the radial current balance in the ASCOT code and, also, in optimizing the code efficiency in the turbulence simulations presented in Publication 5. Especially, the iterative method to simulate the radial electric fields presented in Publication 7 has been developed by the disputant.

Other publications related to this thesis with a contribution by the disputant are Refs. [42, 53, 58, 69].

Contents

Chapter 1

Introduction

The population explosion and an increasing standard of living combine to increase the world's energy consumption. There are many different ways to face this need. Conventional energy sources entail several problems: resources of fossil fuels are limited and they pose a serious environmental threat. As a solution, using renewable energy sources, such as solar and wind energy, is often called for, but until a proper method for energy storage is found, they have limitations due to strong daily and seasonal variations in the primary source of the energy. Earlier, nuclear energy through fission was thought to be the final solution to energy problems because its emissions to air and water are minimal. More recently, however, public opinion has turned against it. Furthermore, like fossil fuels, the fuel of nuclear power plants, Uranium isotope ^{235}U, has limited resources. All such problems can be avoided, if we can exploit fusion reaction rather than fission. Nuclear fusion is considered an environmentally friendly energy source with inexhaustible resources. However, to exploit the reaction, high technology is required, which makes nuclear fusion expensive compared to conventional energy sources. In this thesis, one of the chief problems in nuclear fusion, plasma confinement, is explored.

The goal of controlled nuclear fusion research is to generate energy by combining two low-mass nuclei to form a more massive nucleus. This reaction is the power source of the sun and other stars, where confinement and heating occurs through compression under enormous gravitational forces. Harnessing the energy of stars on Earth sets demanding requirements for temperature, density, and confinement time in order to force positively charged particles to fuse at a rate that makes energy production possible. In order to reach the so-called *break-even*, where the fusion energy released exceeds the amount of energy applied to heating, particles must be confined for a sufficient period at a sufficiently high temperature. A step further is the fusion *ignition*, where the auxiliary heating can be turned off. The ignition is best achieved in reactions with relatively large cross-sections

$$ {}^{2}_{1}\mathrm{D} + {}^{2}_{1}\mathrm{D} \rightarrow {}^{3}_{1}\mathrm{T}(1.01\mathrm{MeV}) + {}^{1}_{1}\mathrm{p}(3.03\mathrm{MeV}) $$

$$^{2}_{1}\mathrm{D} + ^{2}_{1}\mathrm{D} \rightarrow ^{3}_{2}\mathrm{He}(0.82\mathrm{MeV}) + ^{1}_{0}\mathrm{n}(2.46\mathrm{MeV})$$

$$^{2}_{1}\mathrm{D} + ^{3}_{1}\mathrm{T} \rightarrow ^{4}_{2}\mathrm{He}(3.57\mathrm{MeV}) + ^{1}_{0}\mathrm{n}(14.06\mathrm{MeV})$$

$$^{2}_{1}\mathrm{D} + ^{3}_{2}\mathrm{He} \rightarrow ^{4}_{2}\mathrm{He}(3.67\mathrm{MeV}) + ^{1}_{1}\mathrm{p}(14.67\mathrm{MeV}).$$

Here, the lowest threshold for net energy production involves a reaction in which Deuterium (D) and Tritium (T) fuse, producing a helium nucleus (He) and a neutron (n), and, most importantly, releasing energy, which is given in parentheses for each reaction product (p denotes proton). For this reaction, the necessary requirement for the ignition is

$$n\tau_E > 1.5 \times 10^{20}\mathrm{m}^{-3}\mathrm{s},$$

where n is the density, and τ_E is the energy confinement time. The required temperature is in the order of $T = 10^8 K$. If a gas is heated to such a high temperature, it does not remain electrically neutral; electrons are stripped from the atoms. Thus, two populations of oppositely charged particles, electrons and ionized atoms, are formed. This is known as a 'plasma'. Because it is not a solid, liquid, or gas, it is sometimes referred to as the fourth state of matter.

1.1 Fusion devices

Since an extremely high temperature is needed for nuclear fusion, it is obvious that the plasma confinement is not a trivial problem. In *inertial fusion* a dense, hot plasma is produced and confined only for a very short time (nanoseconds) dictated by its inertia. In *magnetic fusion*, the fact that the charged particles in a magnetic field are tied to the field lines is exploited. In linear machines, magnetic field lines end on a material wall. This concept suffers from end losses, although the losses can be decreased by using magnetic mirrors to reflect the particles. In a toroidal device the magnetic field lines are closed, and the problem of end losses is avoided. However, in addition to the motion of particles along the field lines and the gyromotion around the field lines, the particles have a drift velocity in the direction perpendicular to the magnetic field and its gradient. For this reason, the magnetic field consists of a strong toroidal and a weaker poloidal field component, forming helically winding field lines around the torus. The helicity of the magnetic field lines prevents the particles from escaping confinement due to the perpendicular drift. The magnitude of the field varies roughly as $B \propto 1/R$, where R is the distance from the symmetry axis of the torus.

In a *Tokamak*, the poloidal field component is produced by a toroidal plasma current, and the toroidal field component by external coils. The magnetic field is axisym-

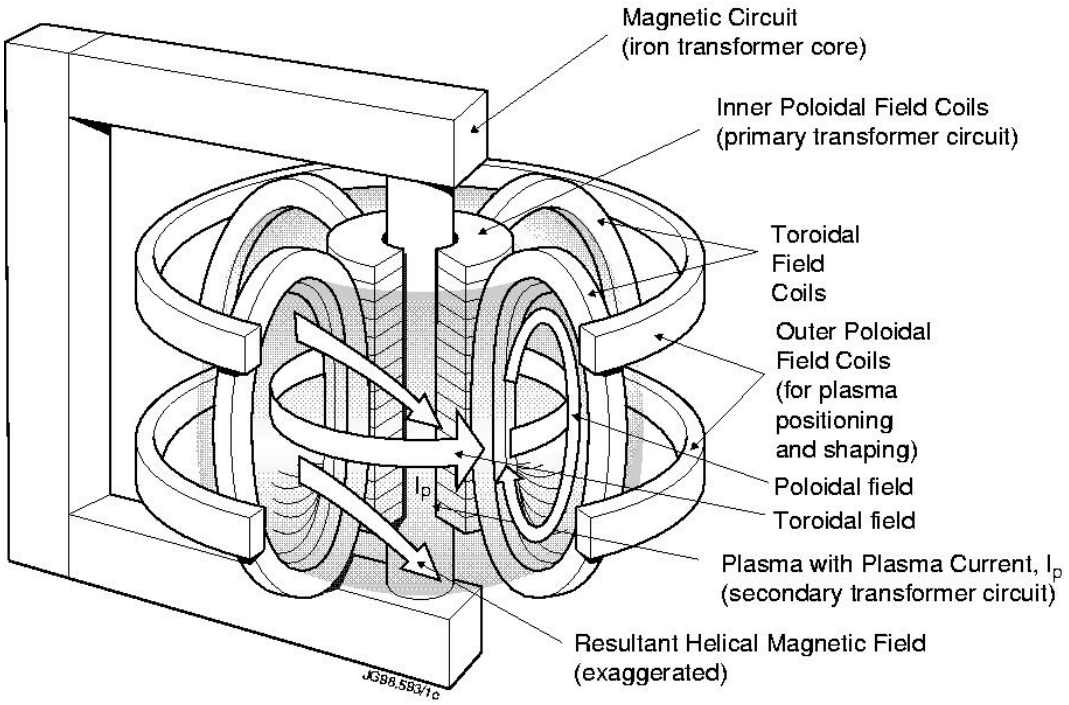

Figure 1.1: *A schematic picture of a tokamak [3]. The toroidal magnetic field is produced by external coils, and the poloidal field by the plasma current I_p.*

metric in toroidal direction, if the small toroidal ripples due to the finite number of field coils are not taken into account. A schematic of a tokamak is shown in Fig. 1.1. In a *Stellarator*, both the poloidal and toroidal magnetic field components are produced by external coils, which leads to a very complicated geometry of the coils. Although a device with closed magnetic field lines guarantees the confinement in parallel direction, Coulomb collisions are always present, inducing particle and heat transport across the magnetic field.

So far the best fusion performance has been obtained in the largest currently existing tokamak, JET (Joint European Torus), in which a transient fusion power of 16.1 MW and a quasi-steady-state fusion power of 7 MW have been obtained [1]. The next-step device ITER (International Thermonuclear Experimental Reactor) is in its design phase [2]. The latest plan for ITER, referred to as ITER-FEAT, is aiming at a gain of $Q \geq 10$ with an inductively driven plasma, and at $Q \geq 5$ in a steady-state. Here, Q is the ratio of fusion power to auxiliary heating power.

1.2 Transport processes

In a toroidal plasma, particle and energy transport result from two different mechanisms. The first one, deriving from Coulomb collisions in toroidal geometry, is referred to as *neoclassical transport* [4], to distinguish it from the classical transport

in cylindrical geometry. Although evaluating the neoclassical transport is mathematically quite difficult, it can be calculated accurately with sophisticated numerical methods, such as orbit-following Monte Carlo codes [5–10]. In a simplified geometry, analytic estimates for the transport coefficients exist under certain approximations [4, 11, 12]. The neoclassical transport theory gives the minimum level of particle and heat flux in a real experiment. However, in recent high performance experiments, transport levels even below the standard neoclassical level have been observed. This calls for revisions in the neoclassical theory [13, 14] to allow for steeper pressure gradients, among other things. In Ref. [15], the revised theory is shown to lead to sub-neoclassical heat fluxes. Also, the validity of the expressions for parallel viscosity and other components of parallel momentum balance equation have been extended to allow for large electric fields observed at the tokamak plasma edge [16, 17].

The second type of transport, known as *anomalous transport*, results from fluctuating electric and magnetic fields which are generally observed in auxiliary heated toroidal plasmas. So far this type of transport has been observed to be dominant. In particular, the electron heat conductivity is found to be $10 - 100$ times higher than the neoclassical value, and also the ion transport and heat conductivity are not sufficiently accounted for by the standard neoclassical theory. In electrostatic turbulence the confining magnetic field is unperturbed, and the transport is driven by fluctuations in the electric field and the fluid quantities. In magnetic turbulence the confining magnetic field is perturbed by current fluctuations in the plasma. Experimental evidence indicates that the electrostatic turbulence dominates [18]. Based on experiments, different scaling laws have been proposed, e.g., 'Bohm' and 'gyro-Bohm' -models, which give the energy confinement time as a function of dimensionless variables [19]. These variables can be, for example, the normalized collisionality ν_*, which gives a measure of collisions during a bounce period, the plasma beta β, which gives the efficiency of confinement, and the normalized gyroradius ρ_*. An adequate analytic theory for the anomalous transport is still missing, but in the numerical modeling of turbulence a lot of progress has been made [20].

Experimentally, the anomalous transport has been found to decrease remarkably in the so-called H–mode, which is described in the next section. In addition to the H–mode also other regimes of enhanced confinement have been found (see a review in Ref. [21]). For example, the so-called VH–mode [22, 23] has many features in common with the normal H–mode, but the energy confinement time can be two times higher than in the H–mode.

1.3 L–H transition

Since its discovery in ASDEX tokamak in 1982 [24], the L–H transition has been observed in many divertor and limiter tokamak discharges, and also in some stellarators. In the L–H transition plasma jumps from the Low (L–) confinement mode into

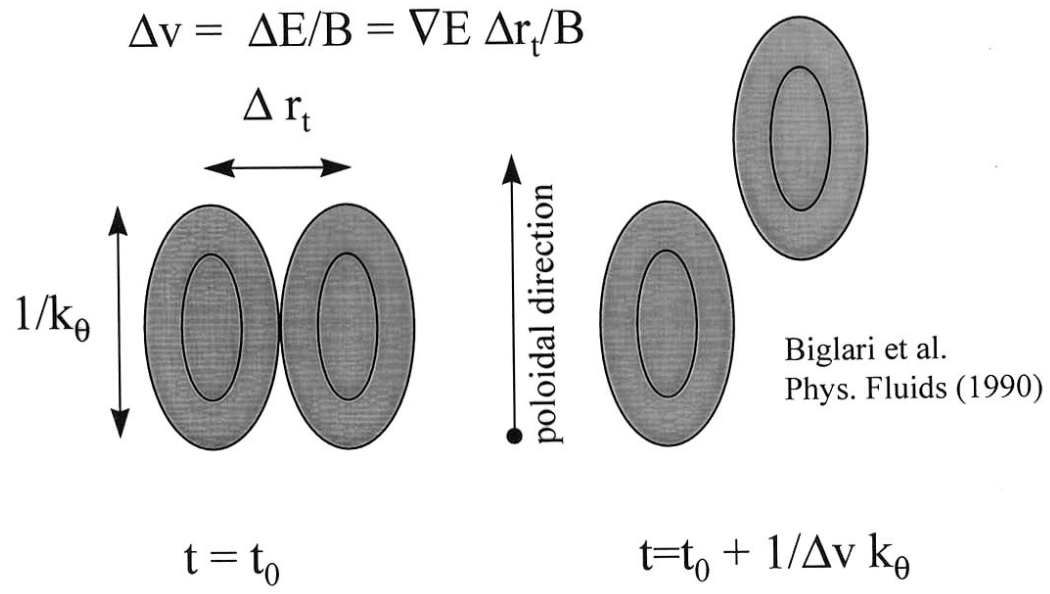

Figure 1.2: *The BDT (Biglari-Diamond-Terry) criterion for the strong suppression of turbulence is* $|\nabla E/B| > \Delta\omega_t/k_\theta \Delta r_t$ *[27]. Here,* $\Delta\omega_t$ *is the turbulent decorrelation frequency,* Δr_t *is the radial correlation length, and* k_θ *is the mean poloidal wave number of the turbulence.*

the High (H–) confinement mode, and the energy confinement time of the plasma is increased by a factor $f_H \approx 2$. An L–H transition is characterized by a threshold in the heating power, which is roughly proportional to the product of the line-averaged electron density $\bar{n}_e$ and the toroidal magnetic field B_t. The power threshold also strongly depends on the direction of B_t. The transition is observed as a reduction of the particle flux out of the plasma.

The leading paradigm for the reduction of turbulent transport in H–mode edge plasma is based on sheared radial electric field. The shear in the radial electric field E_r can reduce transport either through stabilizing the linear modes [25], by reducing amplitudes or correlation lengths of turbulence, or by changing phases between the turbulent fluctuations [26]. In the analytic theory of Ref. [27] a criterion for the strong suppression of turbulence is $|\nabla E/B| > \Delta\omega_t/k_\theta \Delta r_t$ (see Fig. 1.2). If this criterion is satisfied, the radial correlation between neighboring turbulent eddies is effectively suppressed by sheared poloidal rotation. An edge transport barrier, with a width of 1-3 cm, is formed, and fluctuations in magnetic field, density and electrostatic potential are reduced there. Particle diffusivity and heat conductivity are reduced by a factor of 5-10, which for ions means that, in this narrow layer, the transport can be close to its neoclassical value. Although the sudden improvement in confinement has been known for long, the mechanism how the radial electric field is formed in the transition is still unclear. Finding the mechanism for the L–H transition is of great interest because operation in an H–mode allows smaller tokamaks, which is beneficial for developing an economical fusion reactor.

Many models seek for a bifurcation in E_r (or in the poloidal rotation U_θ) in order to explain the fast time scale ($\sim 10^{-4}$s) of the transition. One candidate is the so-called 'Stringer spin-up' [28], in which a bifurcation in the poloidal rotation occurs due to a poloidally asymmetric particle source or transport. Another proposed explanation is based on an asymmetric fluctuation spectrum (Reynolds stress) [29] that causes a flow generation. In both of these cases, the spin-up is assumed to occur due to anomalous processes. In the model of Shaing [30], in which the anomalous processes are not included, the bifurcation arises from a multivalued balance between the ion orbit loss current and the neoclassical return current. At a low edge temperature, the balance occurs for a low value of E_r (the L–mode solution). Heating the plasma will make two stable solutions possible, and a further heating will make the L–mode solution to disappear, causing a bifurcation to a higher electric field value and, hence, to higher $\vec{E} \times \vec{B}$-rotation (H–mode solution). Also, there exist theories in which anomalous transport is assumed to be due to some special mode (e.g. ITG mode [31]), and the transition occurs when this mode is stabilized. In Ref. [14], the neoclassical theory of an impure plasma is extended to allow for steeper density and temperature gradients than usually. There, the possibility of an L–H transition is found due to particle fluxes that are non-monotonic functions of the pressure gradients.

1.4 Outline of this thesis

This thesis is an introduction to and a review of Publications 1–7. In Chapter 2, certain basic neoclassical phenomena are briefly introduced. This includes charged particle motion in a tokamak, the various collisionality regimes, the Fokker–Planck and momentum balance equations, the particle fluxes and parallel viscosity, and the automatic ambipolarity of neoclassical transport. An equation for solving E_r from the current balance is derived, different models arising from this approach are reviewed, and two numerical codes, DEPORA and ASCOT, simulating neoclassical transport quantities, are presented. In addition, a numerical study of neoclassical particle fluxes in the banana regime is carried out using the 3D Fokker–Planck code DEPORA.

In Chapter 3, the principal results of Publications 2–7 are reviewed and discussed. All the simulation results presented in this chapter are obtained using the 5D guiding-center orbit-following Monte Carlo code ASCOT. The importance of the convection and compression terms and the poloidal dependence of density in calculating the total parallel viscosity in high Mach number regime is addressed in Section 3.1. The neoclassical fluxes in the presence of an externally applied E_r are studied in Section 3.2, and a reasonable agreement between the numerical and the analytic results is found over a wide range of Mach numbers and collisionalities. In Section 3.3, as a starting point for a study of current balance, the model of Shaing is investigated by simulating ion orbit loss numerically in realistic ASDEX Upgrade

geometry. In Section 3.4, current balance is simulated by solving all the neoclassical current components at the tokamak plasma edge self-consistently with ASCOT. Simulations are carried out both for ASDEX Upgrade and JET, and the results are compared. At L–H transition conditions, the results show sufficiently high shear for turbulent suppression for both devices although no anomalous current component is included. In addition, the analysis implies a higher threshold shear for ASDEX Upgrade than for JET.

In Chapter 4, the results presented in this thesis are summarized. Also, limitations and further applications of the current approach are discussed.

Chapter 2

Neoclassical theory and radial current balance

In this Chapter, a brief introduction to neoclassical physics is given. First, in Section 2.1, the charged particle motion in a tokamak and the different collisionality regimes are described. In Section 2.2, the Fokker–Planck equation and its first moment, the momentum balance equation, are introduced. These equations describe the collective motion of the particles. Also, the automatic ambipolarity of the neoclassical transport is derived and discussed. When the automatic ambipolarity does not hold, two different approaches can be chosen: First, the particle flux in response to a fixed and maintained E_r can be calculated, or, second, the ambipolar E_r maintaining the current balance can be solved. The knowledge gained from the first approach can be used to facilitate the current balance analysis. Section 2.3 quotes analytic expressions of pressure anisotropy, parallel viscosity and neoclassical return current in response to an externally applied E_r in a collisional plasma. In Section 2.4, an equation for solving E_r from the current balance is derived and different models arising from this approach are reviewed. Two numerical codes simulating neoclassical physics without thin-orbit approximation are presented in Section 2.5.

2.1 Charged particle motion in a torus

A charged particle follows the magnetic field lines only in the first approximation. The gradient of the magnetic field causes ions and electrons to drift perpendicular to the field line (so-called ∇B-drift). For electrons, the effect is smaller by a factor $(m_e/m_i)^{1/2}$. Here, m is the mass of the particle, and subscripts i and e refer to ions and electrons, respectively. Two types of trajectories exist, the passing particle trajectories which rotate around the torus without reversing their direction, and the trapped particle trajectories. The conservation laws for total energy, magnetic moment and toroidal momentum, needed for calculating the trajectories of particle a,

are

$$E_{tot} = \frac{1}{2} m_a v^2 + e_a \Phi = constant, \tag{2.1}$$

$$\mu = \frac{m_a v_\perp^2}{2B} = constant, \tag{2.2}$$

$$P_\phi = m_a R v_\phi + e_a \psi = constant, \tag{2.3}$$

where Φ is the electrostatic potential, v_ϕ and $v_\perp$ are the toroidal and perpendicular components of total velocity v, respectively, $e_a = Z_a e$ is the charge of the particle with the charge number Z_a, and e is the elementary charge. The total magnetic field vector $\mathbf{B} = B_p \mathbf{e}_\theta + B_t \mathbf{e}_\phi$ consists of the poloidal magnetic field component B_p and the toroidal magnetic field component B_t. The coordinate system is chosen so that the unit vectors $\mathbf{e}_\rho$, $\mathbf{e}_\theta$, and $\mathbf{e}_\phi$, showing the radial, poloidal, and toroidal direction, respectively, form a right-handed coordinate system $(\mathbf{e}_\rho, \mathbf{e}_\theta, \mathbf{e}_\phi)$. The poloidal flux $\psi(\rho) = \int R B_p dR$ on a magnetic surface is integrated on the equatorial plane from the magnetic axis outward to the R-value of the surface ρ.

The magnetic trapping of particles results from the conservation of total particle energy and magnetic moment. This makes the particle with a small velocity component parallel to the magnetic field to be reflected at the point of higher magnetic field. In the absence of collisions, a trapped particle bounces indefinitely between the reflection points at the so-called bounce frequency ω_b, which depends on the magnetic field geometry and the properties of the particle. Because of the vertical ∇B-drift, the particle first deviates from its original flux surface and later returns to it. The bounce motion combined with the ∇B-drift leads to so-called banana orbits. Also other types of trapped orbits may exist, e.g., kidney orbits, D-shaped orbits or pinch orbits (see the classification in Ref. [32]).

The deterministic motion of the particles in a tokamak described above is perturbed due to Coulomb collisions with other particles. This leads to the neoclassical diffusion where the term 'neo' refers to the enhancement due to toroidal geometry as compared to the classical diffusion in a cylinder. In standard neoclassical theory, three collisionality regimes are distinguished according to the typical bounce frequency and the ion-ion collision frequency $\nu_{ii} = Z_a^2 e^4 n \ln\Lambda / (4\pi\varepsilon_0^2 m^2 v_T^3)$. Here, $\ln\Lambda$ is the Coulomb logarithm, ε_0 is the vacuum permittivity, $v_T = (2k_B T/m)^{1/2}$ is the thermal velocity of the particle at temperature T, k_B is the Boltzmann's constant, and n is the density of the ions. In order to define the collisionality regimes, it is convenient to adopt the normalized collisionality $\nu_{*i} = \nu_{ii} R q / v_T \epsilon^{3/2} \approx \nu_{ii}/\omega_b \epsilon^{3/2}$. Here, $\epsilon = r/R$ is the inverse aspect ratio with minor radius r, and $q = \epsilon B_t / B_p$ is the safety factor. In the collisional *Pfirsch-Schlüter regime* where $\nu_{*i} > \epsilon^{-3/2}$, a fluid approximation can be used because regular particle orbits in a torus are de-

stroyed by collisions. For weaker collisions, $1 < \nu_{*i} < \epsilon^{-3/2}$, passing orbits exist; this region is called the *plateau regime*. Finally, if $\nu_{*i} < 1$, collisions are very weak, and both passing and trapped orbits exist. This parameter range is known as the *banana regime* because of the presence of banana shaped trapped particle orbits. In the present high performance tokamaks, the bulk plasma is normally in the banana regime, while higher collisionalities, corresponding to plateau and Pfirsch-Schlüter regimes occur near the plasma edge.

2.2 Momentum balance equation and ambipolarity of neoclassical transport

Collective motion of particle species a in axisymmetric toroidal plasmas can be described by the equation

$$\frac{\partial f_a}{\partial t} + \mathbf{v} \cdot \nabla f_a + \frac{e_a}{m_a}(\mathbf{E} + \mathbf{v} \times \mathbf{B})\frac{\partial f_a}{\partial \mathbf{v}} = C_a(f) \tag{2.4}$$

where f_a is a single particle distribution function, i.e. the quantity $f_a(\mathbf{x}, \mathbf{v}, t)d^3xd^3v$ presents the number of particles in the six-dimensional phase space volume element d^3xd^3v at time t. $\mathbf{E}$ is the electric field, $\mathbf{x}$ is the location in the configuration space, $\mathbf{v}$ is the velocity vector. The Fokker–Planck collision operator is $C_a = \sum_b C_{ab}$ where C_{ab} gives the change per unit time in the distribution function for particles of species a due to Coulomb collisions with the particles of species b. A realistic collision operator must conserve particles, momentum and energy. Two examples of numerical codes, DEPORA and ASCOT, using the Fokker–Planck equation are presented in Section 2.5. In DEPORA, the Fokker–Planck collision operator has been used in deriving the transport coefficients, and, in the particle orbit-following code ASCOT, when the fixed background collision model is used, the collision operators are based on a Fokker–Planck operator.

Taking the first two velocity moments of Eq. (2.4), the particle conservation equation

$$\frac{\partial n_a}{\partial t} + \nabla \cdot (n_a \mathbf{u}_a) = 0, \tag{2.5}$$

and the momentum balance equation

$$n_a m_a \frac{d\mathbf{u}_a}{dt} = e_a n_a(\mathbf{E} + \mathbf{u}_a \times \mathbf{B}) - \nabla p_a - \nabla \cdot \mathbf{\Pi}_a + \mathbf{F}_a, \tag{2.6}$$

for the species a are obtained. Here, n_a and $\mathbf{u}_a$ are the fluid density and the flow velocity of the species, respectively. $\mathbf{E} = -\nabla\Phi$ is an electrostatic field, p_a is the scalar pressure, $\mathbf{\Pi}_a$ is the viscous stress tensor, and $\mathbf{F}_a = \sum_b \int m_a \mathbf{v} C_{ab} d^3v$ is the collisional

friction. Following the derivation of Rutherford [33], the automatic ambipolarity of the neoclassical particle transport is here demonstrated. The analysis can be done in a general axisymmetric magnetic configuration, but for simplicity concentric circular flux surfaces are considered. In a quasitoroidal system, the magnetic field can be expressed as $B = (0, B_{p0}, B_{t0})/h$, in which $h = 1 + \epsilon \cos\theta$. Here, the subscript 0 denotes the value at $R = R_0$, and θ is the poloidal angle. In the toroidal component of Eq. (2.6), the pressure tensor can be eliminated by multiplying the equation by h^2 and integrating over poloidal angle, which gives

$$m_a \left\langle h n_a \frac{du_{a\phi}}{dt} \right\rangle = e_a \Gamma_a B_{p0} + \left\langle h(n_a e_a E_\phi^A + F_{a\phi}) \right\rangle \tag{2.7}$$

where $\mathbf{E}^A$ is the applied electric field (due to axisymmetry there is no electrostatic field in the ϕ direction), $\Gamma_a = \langle n_a u_{ar} \rangle$ is the mean radial particle flux with radial flow velocity u_{ar}, and $\langle ... \rangle$ denotes the flux surface average. If an equilibrium is assumed, the left hand side of Eq. (2.7) vanishes. Summing over all particle species, the friction term vanishes due to momentum conservation, and the ambipolarity, $\sum e_a \Gamma_a = 0$, is obtained. This automatic or *intrinsic* ambipolarity is not to be confused with the *ordinary* ambipolarity arising from the quasi-neutrality condition. In the absence of charge sources and sinks, the ordinary ambipolarity holds in all conditions for the total flux, i.e., including also anomalous fluxes [34].

In the derivation of the automatic ambipolarity of neoclassical fluxes three assumptions were made:

1. Plasma is in equilibrium
2. There are no external momentum sources
3. Magnetic configuration is axisymmetric.

If these assumptions are valid, the particle fluxes are independent of the radial electric field (to the order $(r_L/L)^2$), and ambipolarity is 'automatically' guaranteed. Here, r_L is the Larmor radius and L is the gradient scale length. However, in many cases one or more of these assumptions are not valid. Initial state of the plasma with an externally driven poloidal flow may be characterized by arbitrary values of u_θ and toroidal angular momentum. When the external drive is turned off, the poloidal flow is rapidly damped by parallel viscous forces. Two different time scales can be distinguished: the damping time of poloidal rotation τ_p, and the toroidal angular momentum damping time τ_T. Typically $\tau_p \ll \tau_T$, and thus the toroidal angular momentum is constant on the τ_p time scale. The non-ambipolar state terminates in a quasi-stationary state in which the 'ambipolar' E_r is determined by the toroidal angular momentum and the pressure gradient driven diamagnetic flows. An expression for this ambipolar E_r given in the literature is [4]

$$E_r = \frac{T}{e}\left(\frac{n'}{n} + \gamma\frac{T'}{T}\right) + B_p U_\parallel, \tag{2.8}$$

in which $U_\parallel$ is the average parallel flow velocity and γ is a coefficient depending on the collisionality [4]. Derivatives with respect to radius are denoted by the prime and upper case letters $U_x = \langle n(\theta)u_x(\theta)\rangle \,/\, \langle n(\theta)\rangle$ are used for the weighted flux surface averages of the flow velocity components. In the ambipolar state, the mean parallel viscous force vanishes, and the second-order cross-field fluxes are driven solely by the toroidal friction forces. The automatic ambipolarity (independent of the value of E_r) requires time scales $t > \tau_p$, which is implicitly assumed in many transport calculations.

The automatic ambipolarity does not hold in the presence of a biased internal electrode, ion orbit loss current, or other sources or sinks of toroidal momentum [34]. Different expressions predicting the radial conductivity from viscous damping of the poloidal rotation [30, 35–38] have been compared to the probe experiments of TEXTOR in Ref. [39]. In Section 3.2, some of these expressions are tested using the Monte Carlo approach. The requirement of axisymmetry in automatic ambipolarity does not hold in stellarators and, in practice, neither in tokamaks because a finite magnetic ripple is always present. Neoclassical theory of transport processes in these non-axisymmetric toroidal magnetic configurations is reviewed in Ref. [40]. Analytically magnetic ripple has been shown to play a role in the current balance under some conditions and assumptions [41]. However, in numerical simulations its contribution has been shown to be negligible [42].

2.3 Parallel viscosity and neoclassical particle fluxes in response to an externally applied $\mathrm{E_r}$

In this section, some of the analytic expressions [16, 43] existing in the literature for parallel viscosity and neoclassical particle fluxes in the plateau and Pfirsch–Schlüter regime (for a given poloidal rotation) are presented. These expressions are compared to numerical simulations in Chapter 3. In the analytic theory, the non-ambipolar ion neoclassical current and the parallel viscosity are calculated from the Fokker–Planck equation using a simplified collision operator. A quasi-toroidal geometry is used, in which cylindrical coordinates are appropriate and the magnetic field has a $1/R$ -dependence. Both in the approximations of [43] and [16], the collision operator conserves momentum, but only in Ref. [43] the particle number and total energy are conserved in collisions. Actually, the momentum is not conserved exactly because the parallel flow is assumed to be zero, while naturally the plasma would rotate toroidally. In both cases, a simplified BGK model [44] for the collision operator is used, poloidal Larmor radius ρ_p is assumed to be small compared to the scale length L, and the small inverse aspect ratio expansion is used. The steady-state ion

distribution function in response to the thermodynamic forces and electric field is calculated from the kinetic equation for the ions, but no external force required for sustaining the given radial electric field, poloidal rotation and parallel flow velocity is included.

The derivation of the neoclassical return current in Ref. [43] includes poloidal variation of the electrostatic field, density and temperature, and is based on full velocity integrals. The gradient and curvature drifts are included, but finite orbit effects and radial variation of the radial electric field along the particle orbits are neglected. In order to simplify the problem, the poloidal electric field is neglected here. Neglecting the radial dependence of density and temperature, the steady-state neoclassical current in Ref. [45] can be written as

$$j_{NC,str} = -D \,\mathrm{Im}\left[(1+2x^2)^2\Lambda + \frac{(I-1)E_r}{\mathrm{i}r\nu B + E_r}\right], \tag{2.9}$$

where $D = n_0 T_0 \epsilon^2 / 2rB_0$ is related to the diffusion coefficient. Here, n_0 and T_0 are the zeroth-order (no poloidal variation) densities and temperatures, respectively, B_0 is the magnetic field at the axis, and $x = M_p = |E_r/v_T B_p|$ is the poloidal Mach number. The functions I and Λ are defined as

$$I(z) = \frac{1}{(2\pi)^{1/2}} \int_{-\infty}^{\infty} \frac{w}{w - 2^{1/2} z} \exp\left(-w^2/2\right) dw, \quad \Lambda = I[I + 2\mathrm{i}xyI + (1-I)x/z]^{-1},$$

where $z = x + \mathrm{i}y$, and $y = \nu_{*i}\epsilon^{3/2}$.

The standard parallel viscosity in terms of pressure anisotropy reads as

$$\langle \mathbf{B} \cdot \nabla \cdot \mathbf{\Pi}_i \rangle = \left\langle (p_\perp - p_\parallel) \frac{\mathbf{B} \cdot \nabla B}{B} \right\rangle \tag{2.10}$$

where $p_\parallel$ and $p_\perp$ are the parallel and perpendicular components of the pressure, respectively. Using the expressions for $p_\parallel$ and $p_\perp$ given in Ref. [45], the pressure anisotropy can be written as

$$p_\parallel - p_\perp = T_0(2x^2 - 1)n_1(\theta) + \epsilon n_0 T_0 \left[4x^2 + \frac{E_r(1-I)}{\mathrm{i}r\nu B + E_r}\right] \exp(\mathrm{i}\theta), \tag{2.11}$$

where the poloidal dependence of the density $n = n_0 + n_1(\theta)$ is

$$n_1(\theta) = -\epsilon n_0 [1 - (1 + 2x^2)\Lambda] \exp(\mathrm{i}\theta). \tag{2.12}$$

An alternative expression for the pressure anisotropy is given in Refs. [16, 46]

$$p_\parallel - p_\perp = -2\pi^{1/2} I_{ps} n_0 m U_\theta v_T B / B_p \left[\frac{\partial}{\partial\theta}(\ln B) - \frac{2}{3}\frac{\partial}{\partial\theta}(\ln n)\right], \tag{2.13}$$

where $U_\theta = (U_\phi B_p - E_r)/B_t$ is the poloidal flow velocity, and the integral I_{ps} is given in Ref. [46]. The expression for parallel viscosity by Shaing [16, 47] in the absence of temperature and density gradients can thus be written as

$$\langle \mathbf{B} \cdot \nabla \cdot \mathbf{\Pi} \rangle = \frac{\pi^{1/2}\epsilon^2}{4r} n_0 m v_T B I_{ps} U_\theta. \tag{2.14}$$

Note that also the poloidal density dependence was neglected here. This assumption is discussed in Section 3.1. In the regime where Pfirsch-Schlüter effects are weak the radial current can be expressed, to the lowest order in ϵ, in terms of the parallel viscosity as

$$j_{NC,sha} = -\frac{\langle \mathbf{B} \cdot \nabla \cdot \mathbf{\Pi} \rangle}{B_p B} = -xD\pi^{1/2} I_{ps}. \tag{2.15}$$

This expression can be compared to Eq. (2.9).

2.4 $\mathrm{E_r}$ from the radial current balance

The electric field in a tokamak plasma edge can be solved either from Poisson equation

$$\nabla \cdot \mathbf{E} = \sigma/\varepsilon_0, \tag{2.16}$$

where σ is the charge density, or from Ampere's law

$$\nabla \times \mathbf{B} = \mu_0 \mathbf{j} + \varepsilon_0 \mu_0 \frac{\partial \mathbf{E}}{\partial t}, \tag{2.17}$$

where $\mathbf{j}$ is the total current and μ_0 is the vacuum permeability. Since the polarization current is $\mathbf{j}_{pol} = (\sum_a m_a n_a / B^2)(\partial \mathbf{E}/\partial t)$, Eq. (2.17) can be written as

$$\frac{1}{\mu_0} \nabla \times \mathbf{B} = \mathbf{j} - \mathbf{j}_{pol} + \varepsilon_0 \left(1 + \frac{\sum_a m_a n_a}{\varepsilon_0 B^2}\right) \frac{\partial \mathbf{E}}{\partial t}. \tag{2.18}$$

From vector identities one obtaines $\langle \nabla r \cdot \nabla \times \mathbf{A} \rangle = \langle \nabla \cdot (\mathbf{A} \times \nabla r) \rangle = 0$ which holds for any vector $\mathbf{A}$. Thus, by taking the radial component of Eq. (2.18) and averaging it over the flux surface, the polarization equation

$$\frac{\partial E_r}{\partial t} = -\frac{1}{\epsilon_\perp \epsilon_0} \langle j_r - j_{polr} \rangle \tag{2.19}$$

is obtained. Here, j_{polr} and j_r are the radial components of the polarization current and the total current, respectively, $E_r = -(\partial\phi/\partial\rho)\langle\nabla\rho\rangle$ denotes the flux surface averaged radial electric field, and

$$\epsilon_\perp = 1 + \left\langle (n_e m_e + n_i m_i)\nabla\rho/\epsilon_0 B^2 \right\rangle / \langle\nabla\rho\rangle \approx \left\langle n_i m_i \nabla\rho/\epsilon_0 B^2 \right\rangle / \langle\nabla\rho\rangle$$

is the perpendicular dielectric constant. In the last step, typical tokamak plasma parameters with $\omega_{pi}^2/\Omega_i^2 \gg 1$ are assumed. Here, $\omega_{pi} = (n_i e_i^2/\epsilon_0 m_i)^{1/2}$ is the ion plasma frequency, and $\Omega_i = e_i B/m_i$ is the ion gyrofrequency. The steady-state electric field is obtained when the different current components balance each other. Solving E_r using this method means an enhancement of computing speed by factor $(\omega_{pi}/\Omega_i)^2$ when compared to the standard solution of Poisson equation.

There are many different physical processes affecting the radial current balance. In Ref. [48], for singly charged ions, the current balance at a phenomenological level is written as

$$\frac{\partial E_r}{\partial t} = \frac{e}{\epsilon_0\epsilon_\perp}(\Gamma_{e-i}^{anom} - \Gamma_i^{v\nabla v} - \Gamma_i^{lc} - \Gamma_i^{NC} - \Gamma_i^{NC,o} + \Gamma_e^{NC,o} - \Gamma_i^{cx}) \tag{2.20}$$

in which Γ_i^x (Γ_e^x) is the radial flux of ions (electrons) due to some process x. Here, Γ_{e-i}^{anom} is the anomalous contribution, $\Gamma_i^{v\nabla v}$ is the Reynolds stress contribution arising from the global flow, Γ_i^{NC} is the contribution of collisional bulk plasma viscosity coupled to the magnetic field inhomogeneity, Γ_i^{lc} is the ion loss cone flux, and Γ_i^{cx} is the ion loss due to charge exchange. Notations $\Gamma_i^{NC,o}$ and $\Gamma_e^{NC,o}$ are used for the contributions of collisional flux arising from sources other than bulk viscosity, e.g., ripple diffusion, or the contribution of gyroviscosity. Different models consider different terms of Eq. (2.20), and often a bifurcation is sought for. In Itoh's model [49], the ion orbit loss current is balanced by the anomalous viscosity current. The plasma is assumed to rotate in the toroidal direction, but not in the poloidal direction as in the model of Shaing [30]. In Shaing's model a bifurcation due to a multivalued balance between the ion orbit loss current and the neoclassical bulk viscosity current, $\Gamma_i^{lc} = \Gamma_i^{NC}$, is found. In a modification of this theory [50], the loss current is calculated from the fast ion population, and in a recent paper by the same author [41], the bulk viscosity current is balanced by the current due to magnetic ripple. In Refs. [51, 52], a one-dimensional simulation of the shear in E_r has been performed using multi-fluid equations including Γ_i^{lc}, Γ_i^{NC}, Γ_i^{cx}, and also some turbulent effects. All these models assume a circular geometry and many simplifications have been made in evaluating the ion orbit loss current.

In Section 3.4, E_r is solved from the radial current balance with a fully kinetic five-dimensional neoclassical Monte Carlo simulation of the tokamak plasma edge in a realistic ASDEX Upgrade divertor geometry, thus avoiding many of the assumptions made in earlier analytic and numerical fluid approaches. Bifurcation is not found, but the level of shear is sufficient for turbulent suppression although all the anomalous components of the current are neglected. A similar simulation for the limiter

device TEXTOR is done in Ref. [53], including also the current due to neutral friction as well as the probe current. There a bifurcation and a solitary-structured E_r are found. Different mechanisms proposed for the generation of E_r are reviewed in Refs. [48, 54, 55].

2.5 Numerical codes

The neoclassical transport resulting from collisions in an axi- or non-axisymmetric toroidal plasma with an arbitrary cross-section can nowadays be calculated to a good accuracy [4,11,12] as long as the particle drift-trajectories do not deviate significantly from constant-density and constant-temperature surfaces. Also, analytical models making various approximations exist. However, when simulating the transport of fusion products and nonthermal ions, an accurate modeling of drift-trajectories has been found important. This requires heavy numerical computations. There have been at least two approaches to incorporate the finite orbit effects in numerical modeling of neoclassical fluxes. First, the appropriately averaged drift-kinetic equation can be solved with finite differencing. Here, the standard approach has been to average kinetic equation over the flux surface, but more recently an equation for which the averaging is done over the trajetories has been derived [56]. To satisfy momentum conservation, a nonlinear collision operator [4] has to be included. Another approach is the orbit-following Monte Carlo method [5–10] in which guiding-center orbits of individual test particles are followed. If the distribution function is needed, it can be evaluated by averaging over particles in a certain part of phase space. Collisions can be modeled either by using operators derived from the Fokker-Planck terms for fixed background density and temperature profiles, or by using the binary collisions technique [57]. In the latter method the particles are paired randomly in a small cell in the configuration space, and small angle collisions are performed pairwise. The problem with the former model is that the momentum is not conserved. In the latter one a good accuracy requires very costly numerical calculations.

Here, two codes are presented: the Fokker–Planck code DEPORA (Distributions of Energetic Particles using ORbit Averaging), and the guiding-center orbit-following Monte Carlo code ASCOT (Accelerated Simulation of Charged Particle Orbits in a Tokamak), which both can solve neoclassical fluxes in a realistic geometry using magnetic background from an experimental data base, and which are not limited by the thin orbit approximation. However, DEPORA is valid only in the collisionless parameter regime. Also, the boundary between the confined orbits and the loss orbits is inconvenient in DEPORA, because the distribution function is simulated in a finite multi-dimensional grid. Consequently, ASCOT is a better tool for solving the neoclassical current balance at the tokamak plasma edge which often is in the collisional regime. However, for solving neoclassical particle and heat fluxes further inside in a low collisional plasma DEPORA needs less CPU resources to obtain accurate results.

2.5.1 Fokker-Planck code DEPORA

Using a formalism based on noncanonical variables, a three-dimensional nonlinear kinetic equation for the low-collisionality axisymmetric tokamak plasmas was obtained in Ref. [56]. The method allows treating large drift-trajectory widths and large inverse aspect ratios, conserves momentum in collisions, and is suitable for computer modeling of neoclassical transport of thermal and nonthermal distributions. Non-Maxwellian distributions are important, in particular, when plasma heating and current drive, or the effects due to energetic fusion products are studied.

Assuming that the particle motion is fast compared to Coulomb relaxation time, the kinetic equation can be averaged over the gyroangle, poloidal angle and toroidal angle. This, however, limits the validity of the method to the banana regime. Under this approximation, the evolution of the distribution function of the charged particles can be solved in three dimensions using the so-called constants-of-motion (COM) coordinates. Each set of COM coordinates corresponds to a certain trajectory. In an axisymmetric tokamak, the trajectories are completely characterized by the constants of motion equations (2.1)–(2.3). The kinetic equation with Coulomb collision terms is averaged over these trajectories, not over the flux surface. In these coordinates, the nonlinear kinetic equation can be written as [56]

$$\frac{\partial f}{\partial t} = \frac{1}{J} \sum_{n=1,2,3} \frac{\partial}{\partial \bar{x}^n} \left[\sum_{m=1,2,3} \left(A_{nm} \frac{\partial f}{\partial \bar{x}^m} \right) + B_n f \right], \tag{2.21}$$

where $\bar{x}$ refers to COM coordinates, J is the Jacobian, and the collisional coefficients A_{nm} and B_n are given in [56].

In DEPORA, Eq. (2.21) is solved using finite differences. What makes DEPORA special as compared to the earlier approaches [32,56] is the novel choice of the COM coordinates, which enables an easier treatment of the trapped-passing boundary (TPB). For the 'good' set of the constants of motion, it is required that: a) the coordinates should be physically meaningful, b) the representation should be unique in the sense that a given point in the COM space corresponds to one and only one orbit, and c) the phase space should be well-filled [32]. In order to avoid the problems of the coordinates used in Refs. [32,56], the choice of COM coordinates for DEPORA is done with special care. The coordinates γ_0 and v_0 are chosen as in Ref. [56], i.e., γ_0 is the flux surface label at the innermost point of the drift trajectory for the passing particles and at the bounce point for the trapped particles, and v_0 is the speed corresponding to the total energy of the particle including the electrostatic potential. For the third COM-coordinate we have chosen

$$\lambda = \begin{cases} \zeta^i(B_{max}, \theta^i = \pi), & \text{for passing particles;} \\ \theta^i(B_{max}, \zeta^i = \frac{\pi}{2}), & \text{for trapped particles,} \end{cases}$$

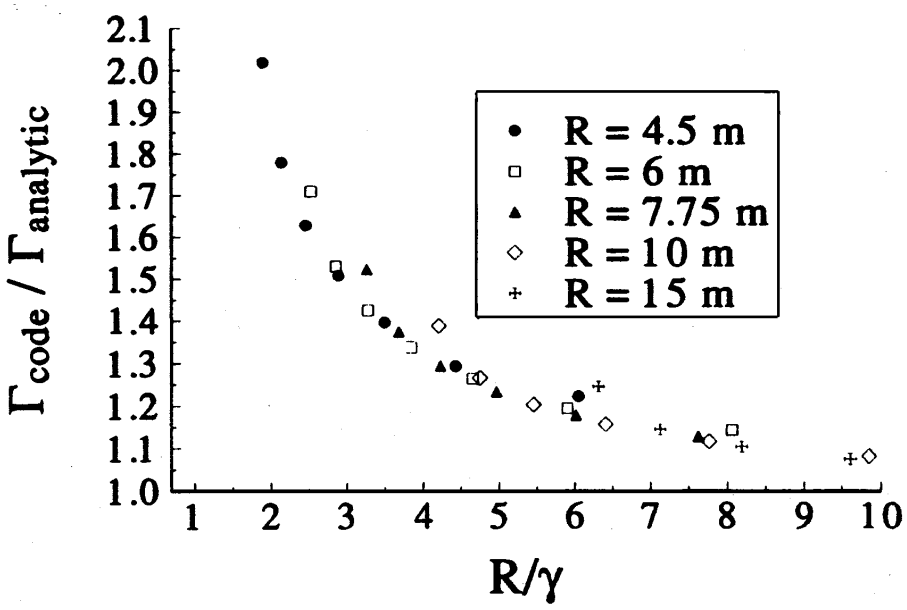

Figure 2.1: *Ratio between numerical and analytic result as a function of aspect ratio*

which corresponds to the pitch angle ζ^i in the *innermost* point of the trajectory for passing particles, and the poloidal angle θ^i at the bounce point for trapped particles. With this choice, the requirement of the well-filled space is satisfied, as shown in Publication 1. Also, the treatment of the trapped–passing boundary is simpler, because γ_0 and λ are defined at the same point, and both are continuous across TPB. With the present coordinates, TPB is independent of γ_0 and v_0, which makes the differencing straightforward.

The performance of the code and limitations of the analytic theory have been tested by comparing the fluxes calculated by the code to the analytic estimates in the banana regime [56]. In the simulation, parameters $a = 2.8$ m, $B = 6.157$ T, and $I = 15$ MA are chosen. Electric field is here neglected. The plasma density and temperature are $n, T = n_0, T_0 \times (1 - \gamma^2/a^2)^{0.5}$ with $n_0 = 0.4 \times 10^{20}$ m^{-3} and $T_0 = 10$ keV. Grid size is chosen so that the further increasing the number of grid points changes the results less than two percents. In Fig. 2.1 the major radius R and the radial coordinate γ are varied. The analytic and numerical results are in a good agreement for large aspect ratios, but for $R/\gamma \leq 5$ the analytic flux strongly underestimates the true flux obtained from the numerical simulation. Thus, the validity of the large aspect ratio approximation in analytic theory is shown to be clearly limited.

A more detailed description of the code is given in Ref. [58] and in Publication 1.

2.5.2 Orbit-following Monte Carlo code ASCOT

The Monte Carlo guiding-center orbit-following code ASCOT [59,60] is a 5D (3D in configuration space and 2D in velocity space) code, which can be used in a numerical simulation of neoclassical physics. Because this thesis concentrates on neoclassical fluxes, viscosity, and radial current balance, only those properties of ASCOT which play a role in these simulations are described here. In addition to the quantities simulated in this thesis, ASCOT has been used to study problems such as the reverse runaway phenomenon [61], radio frequency heating and current drive of both electrons [62] and ions [60], the internal transport barrier physics and the effect of magnetic ripple [42], just to mention a few applications.

The flow chart of the ASCOT code is shown in Fig. 2.2. The initialization of the ion ensemble can be done according to the assumed background density and temperature. The test particles are distributed uniformly in radius, and in poloidal and toroidal angle. The weight factors assigned to the test particles are proportional to the total particle number contained in the initialization volumes, and thus reflect the density profile. In the velocity space the particles are distributed evenly in the particle pitch $v_\parallel/v$, and randomly in speed according to a Maxwellian distribution that corresponds to the local temperature. The guiding-center orbits of the test ions are followed in a tokamak geometry. These equations are written in straight magnetic field line coordinates [63] using canonical Hamiltonian variables to avoid numerical drifts. However, outside the separatrix the conventional Cartesian coordinate system is used. The magnetic background is assumed stationary. For each individual particle, the total energy, magnetic moment and toroidal momentum remain constant in the Runge-Kutta integration of the orbit, but they are altered in collisions. For a group of particles in each spatial cell, however, these quantities are conserved in collisions if the binary collision model [57] is used for ion-ion collisions. In some problems, collisions with a fixed Maxwellian background are appropriate although in that case momentum is not conserved. The electric field can be constant in time, or it can be solved self-consistently from the collective motion of the test particles. If the self-consistent model is used, the net radial motion of the test particle ensemble in the presence collisions, guiding-center drifts, ion orbit losses and gyroviscosity is first evaluated. Then, assuming that electrons provide a stationary background, the change in E_r is solved from the evaluated ion flux using Eq. (2.19). The details of the self-consistent evaluation of E_r can be found in Section 3.4.1.

In problems where neither the binary collision model nor the self-consistent E_r calculation is used, the test particles can be followed one by one until the end of the simulation time since the particle interaction rates do not depend on the motion of the other particles. Otherwise, the simulation time t_{max} is divided in ensemble time steps Δt_{ens} and all particles are advanced along their guiding-center orbits over this time before the next ensemble time step. A new value for electric field is calculated and/or small angle collisions are performed in the entire test particle ensemble after each Δt_{ens}. An ensemble time step is typically only a small fraction ($\sim 1/100$) of the

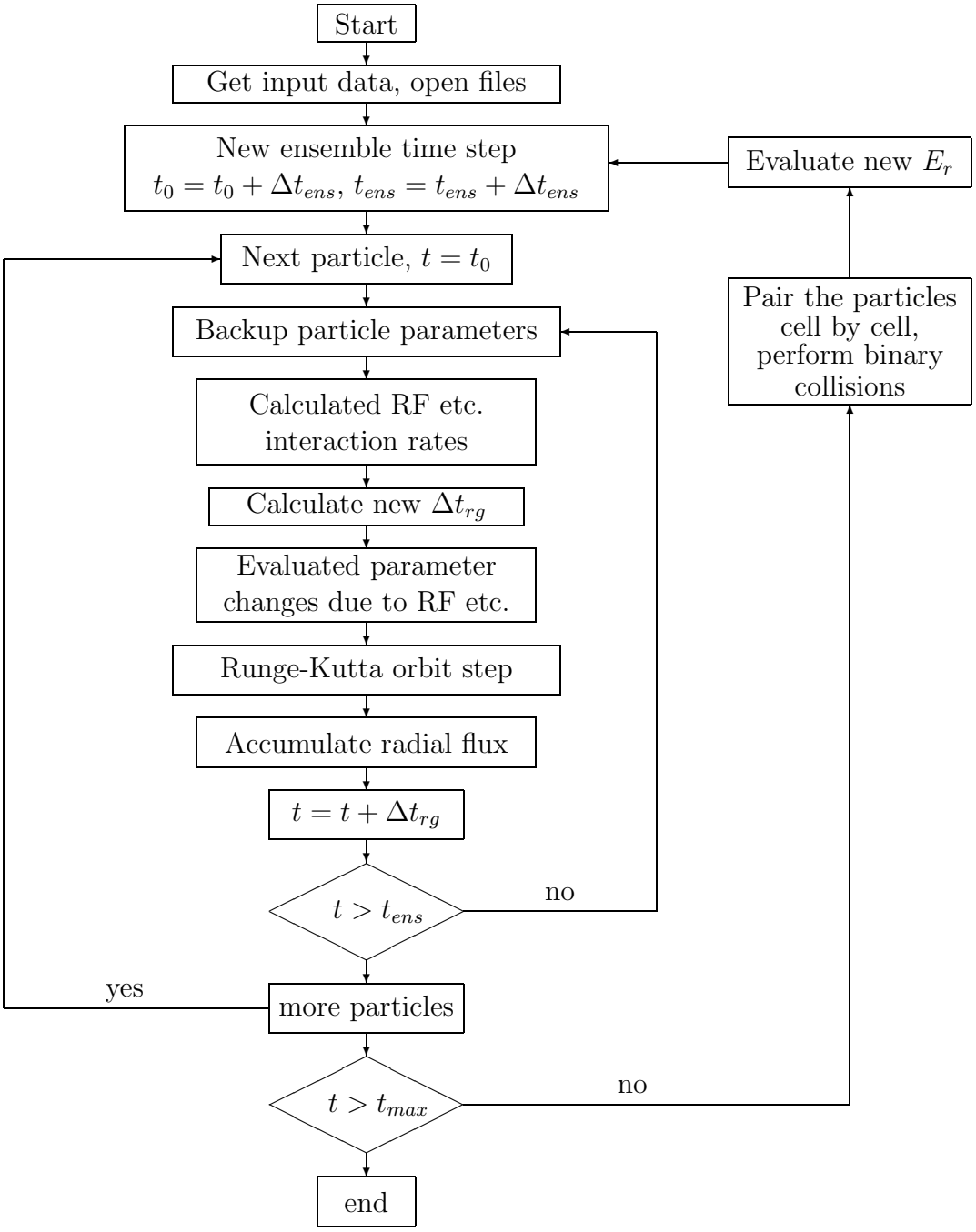

Figure 2.2: *The flow chart of the ASCOT code. The outermost loop is performed only in simulations where the binary collision model and/or self-consistent E_r model is used. At each ensemble time step, all test particles are followed over a time Δt_{ens} which may consist of one or more Runge-Kutta steps Δt_{rg}. Typically, $t_{max} > \tau_c \sim \tau_b > \Delta t_{ens} \geq \Delta t_{rg}$.*

collision time $\tau_c = \nu_{ii}^{-1}$ and the bounce time $\tau_b = \nu_b^{-1}$. Since a relatively small time step and a huge number of particles are often needed, the code has been parallelized using the MPI standard to get simulation results in a reasonable time.

As mentioned above, two different collision models can be used in ASCOT, either the binary collision model or the model in which collisions are performed with a fixed Maxwellian background. In the binary collision model, the simulation region is divided into cells (in r and θ) small enough so that the plasma parameters are approximately constant inside the cell. In each cell, particles are paired randomly and they are collided pairwise. When using this model with a fixed E_r and in the absence of other forces, a test particle flow parallel to the magnetic field arises to compensate the $\mathbf{E}\times\mathbf{B}/B^2$ and the diamagnetic poloidal rotation. If only like-particle collisions are included, this results in a zero radial particle flux in a stationary state. If E_r is solved self-consistently, then the zero radial flux results from the change in E_r and this happens in a faster time scale than the changes in parallel rotation.

The binary collision model is more rigorous but also heavier to run. Thus, in problems where it is not necessary to use the momentum conserving model (e.g., in the simulation of minority ions), collisions with the fixed background are appropriate. As shown in Publication 2, the fixed background collision model can also be used as a parallel force to support stationary solutions with nonzero rotation in calculating the radial current. This was verified by comparing the results of the fixed background collision model with the simulations done using the binary collision model. Both methods give initially the same radial ion flux, but after that, in the momentum conserving case, the parallel velocity develops and the flux decays. Also, when the radial current balance at the tokamak plasma edge is simulated, collisions with the fixed background can be used to maintain the temperature profile in longer runs. Otherwise, with the full collision operator, the plasma starts to cool as the hot ions lost to the wall are replaced by thermal ions. In Publication 6, the two collision models are shown to produce the same E_r profiles from the current balance in shorter runs, where the temperature does not have time to change significantly.

Chapter 3

Simulation of neoclassical fluxes, viscosity and current balance

In present tokamaks, the radial transport due to anomalous processes clearly exceeds the neoclassical transport. However, the latter may play a dominant role in advanced confinement regimes, such as in the case of internal transport barriers or H–mode. Indeed, the transport levels near, or even below [64], the standard neoclassical level have already been observed in some experiments. For this reason, verifying of the analytic expressions for the neoclassical fluxes is important. Also, the neoclassical component can be relatively significant in the radial current balance. E_r and its shear can be determined from this balance and, if the balance is multi-valued, a bifurcation may occur. In the model of Ref. [30], the balance between the non-ambipolar loss of fast ions and the return current is studied and a bifurcation is found. Thus, the numerical study of both of these current components as a function of various parameters, such as radial electric field and collisionality, is of interest. However, since the ion orbit loss current and the neoclassical return current consist of the same current carriers, and since, in practice, the separation of these two is impossible, a self-consistent test particle simulation of the edge plasma gives the most reliable result. The anomalous current component is neglected here since it is relatively small at least in the case of electrostatic fluctuations [65].

In all numerical work presented in this chapter, the 5D guiding-center orbit-following Monte Carlo code ASCOT (presented in Section 2.5.2) is used. In Section 3.1, the qualitative behavior of the bulk viscosity is shown to be inaccurate in earlier analytic treatment [47] for high M_p due to the neglect of poloidal dependence of density. The importance of the convection and compression terms in that regime is shown. In Section 3.2, the neoclassical fluxes in the presence of an externally applied E_r are studied over a wide range of Mach numbers and collisionalities. Reasonable agreement between the numerical and analytic result is found. In Section 3.3, the ion orbit loss current as a function of collisionality is simulated within the framework of Shaing's model. The analysis is a simplified version of the current balance. Similar

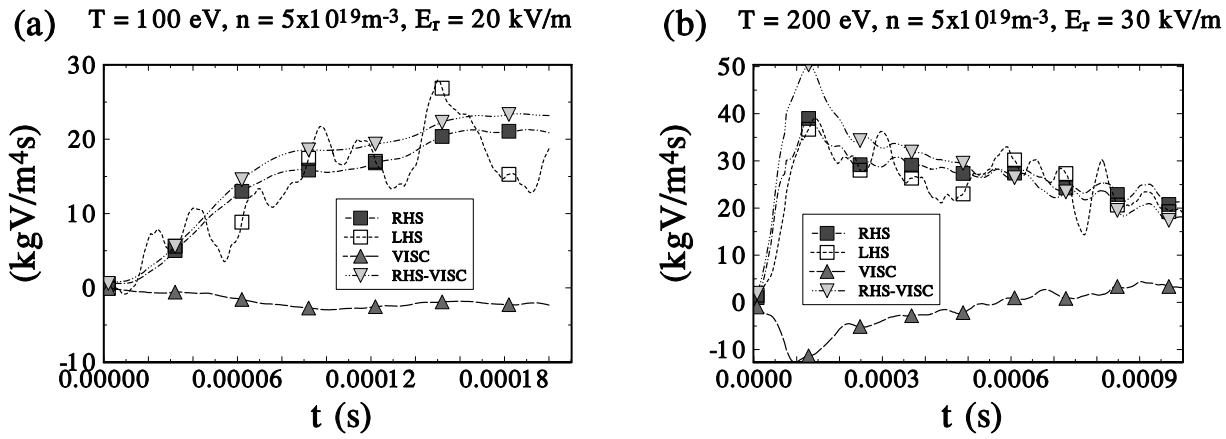

Figure 3.1: *The LHS and RHS of Eq. (3.1) are compared for two different temperatures and E_r. In figure, RHS is also separated to the standard parallel viscosity term (VISC) and to the sum of other terms (RHS-VISC). The time derivative is sensitive to the noise due to the finite number of test particles.*

assumptions are done as in the analytic theory and, thus, also the results are similar. In Section 3.4, the neoclassical current balance is simulated self-consistently. The shear in rotation is found high enough for significant turbulent suppression.

3.1 Parallel viscosity in collisional regime

Assuming that the electric field is electrostatic and that there are no other external forces, one can take an inner product of Eq. (2.6) with $\mathbf{B}$ and, after the flux surface averaging, the equation for the ion parallel flow dynamics reads

$$\left\langle m_i \frac{\partial (n_i \mathbf{B}\cdot\mathbf{u}_i)}{\partial t} \right\rangle = -\langle \mathbf{B}\cdot\nabla\cdot\mathbf{\Pi}_i\rangle - \langle m_i(\mathbf{B}\cdot\mathbf{u}_i)\nabla\cdot(n_i\mathbf{u}_i)\rangle - \langle n_i m_i \mathbf{B}\cdot\mathbf{u}_i\cdot\nabla\mathbf{u}_i\rangle\,, \tag{3.1}$$

where the right hand side (RHS) can be interpreted as the total parallel viscosity consisting of the standard parallel viscosity and convection terms valid for arbitrarily large center-of-mass velocities. In this section, the standard parallel viscosity and other components of Eq. (3.1) are studied numerically. These are calculated directly from the ASCOT code in terms of the averaged parallel and perpendicular flow velocities, $u_\parallel$ and $\mathbf{u}_\perp$, and the pressure components $p_\parallel = \int m(v_\parallel - u_\parallel)^2 f d^3v$ and $p_\perp = \int [m(\mathbf{v}_\perp - \mathbf{u}_\perp)^2/2] f d^3v$, respectively. All the flow velocity components as well as $p_\parallel$ and $p_\perp$ are calculated in the code as time and ensemble averages of the particle velocities. Results are compared to the viscosity given by Eq. (2.14).

In the numerical simulation, a circular symmetry with no Shafranov shift is assumed, consistent with the assumptions made in deriving the analytic forms. Viscosity is determined at the radius $r/a = 0.5$, and to ignore the influence of gradients, temperature, density and current density profiles are assumed to be flat. Parameters

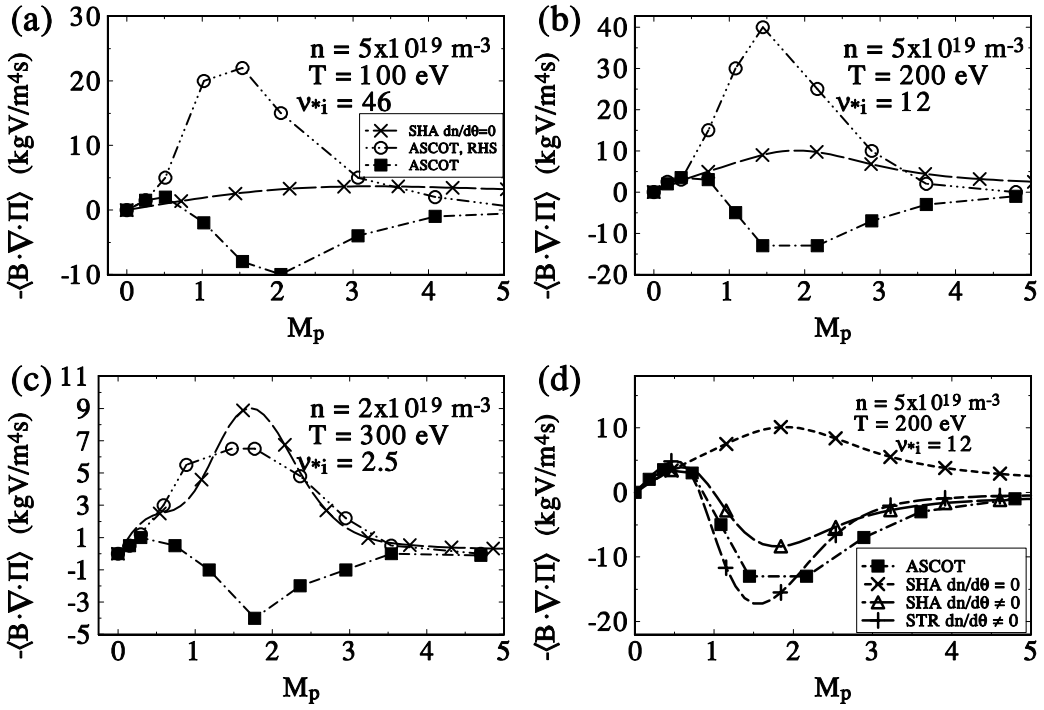

Figure 3.2: *Parallel viscosity as a function of M_p for collisionalities a) 46, b) 12 and c) 2.5 calculated with ASCOT and from the expression of Shaing, and the sum of RHS terms in Eq. (3.1) calculated with ASCOT. In Fig. d) the case b) is redrawn, but now using the pressure anisotropies of Eqs. (2.13) (SHA) and (2.11) (STR) with poloidal density dependence of Eq. (2.12) in analytic formula.*

similar to those of ASDEX Upgrade, $a = 0.5$ m, $I_p = 1$ MA and $B_t = -2.5$ T, are used for minor radius, plasma current and toroidal magnetic field on the axis, respectively. The major radius, however, is chosen to have a larger value ($R = 3$ m) to neglect the effect of small aspect ratio corrections (the analytic results were derived in the large aspect ratio limit).

It is important to notice that E_r is not allowed to develop. Thus, the changes in U_θ are not due to changes in E_r, but due to toroidal rotation which starts to develop because the momentum conserving binary collision operator is used (see the discussion of the different collision models in Section 2.5.2). Thus, the time scale is τ_T rather than τ_p. As a test of the performance of the code, in Fig. 3.1, the LHS (left hand side) and RHS of Eq. (3.1) are compared for two different collisionalities. Within the accuracy of the simulation, the results agree. Noise due to finite number of test particles causes inaccuracy especially in the time derivative which can be seen in the figure. To investigate the relative importance of the standard parallel viscosity term $\langle \mathbf{B} \cdot \nabla \cdot \mathbf{\Pi}_i \rangle$ (VISC), and the other RHS terms (RHS-VISC), these are separated in the figure. Here, the RHS of Eq. (3.1) is the total parallel viscosity, and (RHS-VISC) includes convection and compressibility terms. It is shown that the convection and compressibility terms, which are neglected in many analysis, indeed dominate the time behavior. In Fig. 3.2, to further study the importance of these terms, the numerically obtained total parallel viscosity is compared to the

standard parallel viscosity calculated numerically from Eq. (2.10) and analytically from Eq. (2.14) as a function of M_p. Here, the density is $n = 5 \times 10^{19}$ m^{-3}, and temperatures a) 100 eV and b) 200 eV correspond to the collisionalities $\nu_{*i} = 46$ and 12, respectively, the first one being in the Pfirsch-Schlüter regime and the latter in the plateau regime. The evaluation is done transiently after the initialization effects have been wiped away, but before any significant parallel velocity develops. Choosing a right time instant introduces an inaccuracy which can be $20 - 30\%$. Both in the Pfirsch-Schlüter regime and in the plateau regime, for large poloidal Mach numbers, the standard parallel viscosity has a opposite sign than the sum of all RHS terms, i.e., its effect is to resist the growth of the parallel rotation which is driven by the other terms. With small poloidal rotation, also the standard parallel viscosity drives parallel rotation which leads to the decay of the poloidal rotation. For small M_p, a good agreement between the numerically obtained standard parallel viscosity and the analytic result is found in plateau regime. In Fig. 3.2c, the same comparison is made for the low collisionality case, i.e., for temperature $T = 300$ eV with density $n = 2 \times 10^{19}$ m^{-3} corresponding to a collisionality of $\nu_{*i} = 2.5$. Again, we find that the parallel viscosity from the simulation changes sign for large poloidal Mach numbers but, somewhat surprisingly, a fairly good agreement can be found between the Shaing's expression for the standard parallel viscosity and the ASCOT result for the total parallel viscosity.

The reason for the qualitative difference arising in standard parallel viscosity at high poloidal Mach numbers is the strong poloidal density dependence that develops for large M_p and is neglected in Ref. [47]. If the poloidal density dependence of Eq. (2.12) is taken into account in the analytic expressions of pressure anisotropy of Eqs. (2.11) and (2.13), the analytic theory agrees qualitatively with the numerical simulation. This is shown in Fig. 3.2d and is further discussed in Publication 3. However, one should note that, the qualitative behavior of the viscosity term in Ref. [17], defined as $\langle \mathbf{B} \cdot \nabla \cdot \mathbf{\Pi}_i / n \rangle$, is different (no change in sign) from the behavior of the standard parallel viscosity $\langle \mathbf{B} \cdot \nabla \cdot \mathbf{\Pi}_i \rangle$.

3.2 Neoclassical particle fluxes as a response to externally applied $\mathrm{E_r}$

Several analytic expressions for the neoclassical return current have been derived that are valid for different collisionality regimes and under various assumptions. In numerical simulations, many of the simplifications adopted in theory are unnecessary, e.g., a more complete collision operator can be used. Here, the neoclassical current obtained with the ASCOT code is compared with the analytic expressions given by Eqs. (2.9), and (2.15). The simulation is done as a function of M_p for several collisionalities varying the temperature and density. Other parameters are the same as in the previous section. The nonambipolar flux surface averaged ion radial current density due to a fixed radial electric field E_r is simulated by accumu-

lating the net radial ion motion of the test particle ensemble in ASCOT. The flux is determined at the radius $r/a = 0.5$.

Figure 3.3 shows the return current from ASCOT and from the analytic expressions as a function of the poloidal Mach number M_p for normalized collisionalities $\nu_{*i} = 49$, 45, 23, 9.4, 6 and 2.5. Collisionality is varied by changing both the temperature and the density (values are given in the figures). Qualitatively the results agree, and quantitatively the results are of the same order. It can be seen that the agreement between different approaches depends on collisionality and the best fit is obtained in the middle of plateau regime. The location of the maximum of the current in Eq. (2.15) by Shaing strongly shifts to higher values of M_p when collisionality is increased, but for the current in Eq. (2.9) by Stringer, the maximum is at $M_p \approx 1$ for all cases. The latter is in better agreement with the numerical results which show only a small shift of the maximum. When the bifurcation model of Ref. [30] is considered, the collisionality regime near the limit of banana regime ($\nu_* = 1$) is the most interesting. As can be seen from Fig. 3.3f, near the banana limit Shaing's result and ASCOT simulation give a nearly equally high maximum meaning that Eq. (2.15) gives a reliable estimate in the regime relevant for bifurcation analysis.

Some of the differences obtained here may be explained by the different collision models used. In derivations of Eqs. (2.9)–(2.15), essentially the Krook model [12] (in a somewhat modified form) for collisions was applied. Although with proper coefficients the Krook model is known to reproduce viscosity and fluxes obtained from a more complete collision operator in a relatively wide collision regime for weak rotation, in the present case of large poloidal Mach numbers its validity is not guaranteed. The main difference between Shaing's and Stringer's expressions is most probably that only the latter one is based on full velocity integrals, which might be the reason why it has a tendency to agree better with the numerical results that also take into account the whole velocity space. As in the present work, also in experiments in TEXTOR [39] the return current was found to be between the expressions of Shaing and Stringer. There, an externally biased electric field was introduced with a probe.

3.3 Ion orbit loss current

In Section 2.4, the current balance was considered on a phenomenological level by separating different current components although they are produced by the same current carriers. Different theories concentrate on different components of this balance. As a starting point for a study of the current balance, the model of Shaing is first adopted, but now the ion orbit loss is simulated more accurately. The orbit loss current is usually calculated in a cylindrical geometry, and a number of approximations are made to obtain an analytically tractable system. Here, the Monte Carlo calculations of the orbit loss current are performed in a realistic geometry and experimental data is used as input. The ion orbit loss rate can be determined

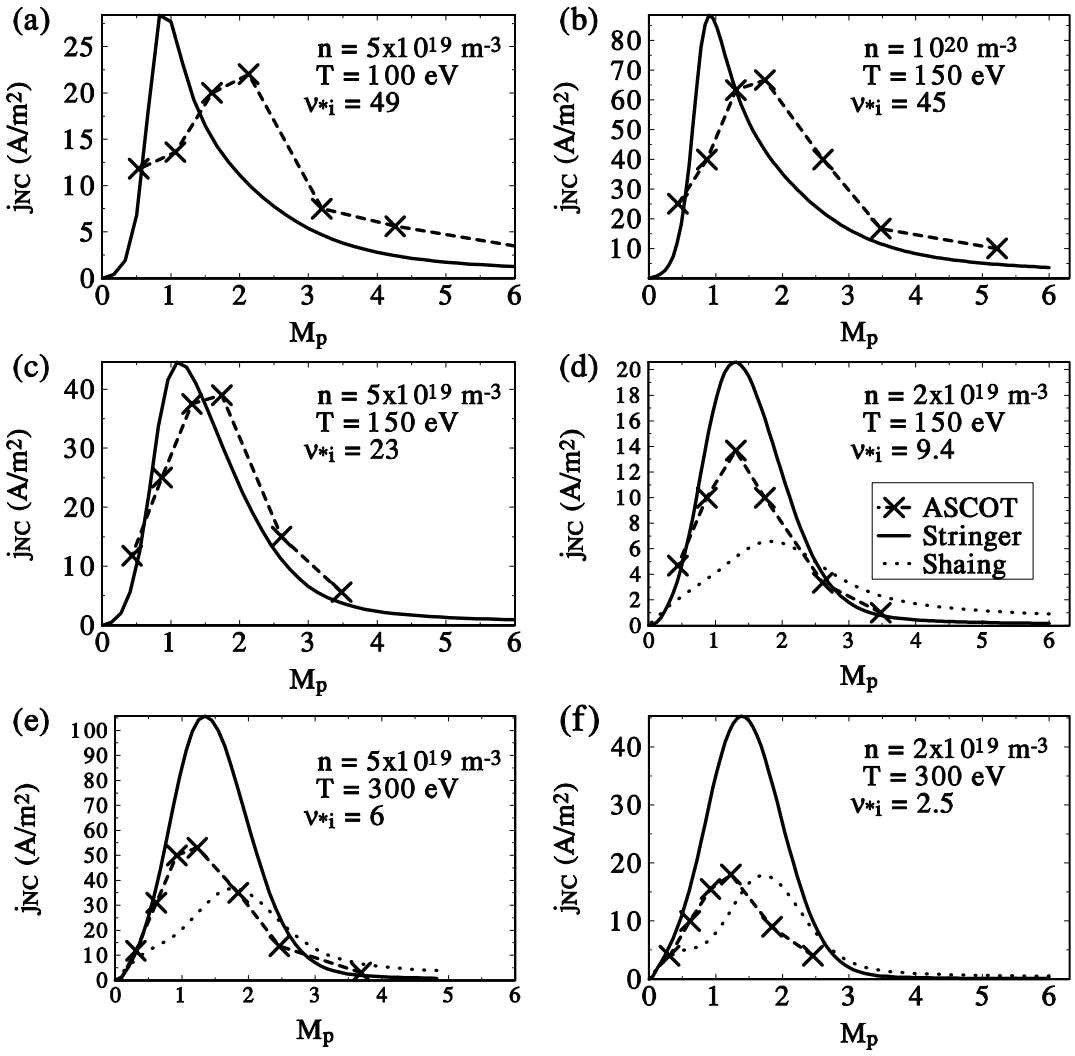

Figure 3.3: *Neoclassical current j_{NC} as a function of poloidal Mach number for various collisionalities. Here, the dashed line with crosses is the ASCOT result, dotted line (shown only for lowest ν_{*i}) is calculated from the expression of Shaing, and solid line from the expression of Stringer.*

accurately because actual particle orbits in a tokamak are followed. The loss cone is determined from the condition that the orbit intersects either the divertor plates or the wall structure. Temperature and density profiles are taken from the experiment, and the collisionality is varied by scaling the temperature. Because the aim is to simulate the orbit losses within the model of Shaing, an external force is required to damp the toroidal rotation. In our model, this external force is provided by the ion-ion collision operator which does not conserve momentum. The current obtained is compared to the neoclassical return current, which is calculated analytically in a circular geometry using Eq. (2.15). However, one should note that fluid parameters are here computed within a regime $\propto \rho_p$ from separatrix although only the kinetic approach would be rigorously justified [55].

In this simple, heuristic model, the ambipolar and non-ambipolar ion orbit losses are separated using specific criteria: Only those escaping particles that cross the equator outside the separatrix only once and are sufficiently collisionless, i.e., $\nu_i/\nu_b < p_c$, when they cross the separatrix, contribute to the non-ambipolar ion orbit losses. Here, p_c is of the order of unity, and $\nu_b = \omega_b/2\pi$ is the bounce frequency. Ions that have $\nu_i/\nu_b \gg 1$ at the separatrix are expected to be accompanied with an almost equal electron flux across the separatrix, while for the ions with $\nu_{ii}/\nu_b < 1$, the radial separation of the ion and electron orbits creates the non-ambipolarity. Here, $\nu_i = \sum_j \nu_{ij}$ is the pitch collision frequency of the ion species i with the background particle species j. From the accumulated number of lost particles, loss current density can be determined as the accumulation velocity divided by the flux surface area.

In the model of Shaing, a necessary condition for bifurcation is that the non-ambipolar ion orbit loss current j_L exceeds the maximum of the neoclassical return current $j_{NC,max}$. In Fig. 3.4a, the loss current j_L from the simulations and j_{NC} from analytic theory, are compared at experimental L–H transition conditions. It is assumed that j_L does not vary as strongly with E_r as the return current does, and that $j_L(E_r = 0)$ gives the largest loss as in the analytic theory [30]. Thus, j_L is simulated only for $E_r = 0$, but j_{NC} is calculated as a function of E_r. In the simulation, ASDEX Upgrade parameters for discharge #8044 at time of the L–H transition are used (see Table 1 in next section). The ion orbit loss is much smaller than $j_{NC,max}$, meaning that the model is unable to explain the bifurcation at these plasma parameters.

In Fig. 3.4b, the loss current $j_L(E_r = 0)$ is presented as a function of ν_{*i} (by scaling the temperature), and compared to the maximum value of the neoclassical return current. At $\nu_{*i} = 3.8$, which corresponds to real experimental ASDEX Upgrade data, the ion orbit loss is much smaller than $j_{NC,max}$, as already shown in Fig. 3.4a. Decreasing collisionality increases the ion orbit loss, and at the same time $j_{NC,max}$ decreases. In the figure, in the banana regime ($\nu_{*i} < 1$), $j_L > j_{NC,max}$ which means that, according to the model, the L-mode solution disappears. In fact, the simulation presented here is in agreement with the analytic model, which shows bifurcation for the normalized collisionality $\nu_{*i} \approx 1$, which is much less than the collisionalities

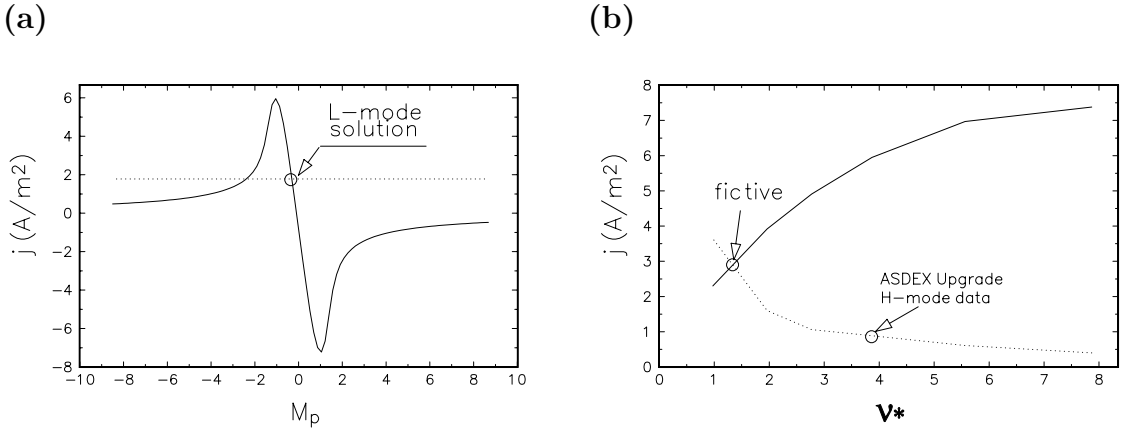

Figure 3.4: *a) The ASDEX Upgrade geometry is used in the numerical calculation of the ion orbit loss current j_L (dotted line). The neoclassical return current j_{NC} (solid line) is calculated analytically in circular geometry. In steady-state, the currents balance each other. b) j_L for $E_r = 0$ (dotted line) and $j_{NC,max}$ (solid line) as a function of ν_{*i}. Bifurcation in the model occurs when j_L exceeds $j_{NC,max}$. By scaling up the temperature, we see that this would happen at $\nu_{*i} \approx 1$.*

observed in the L–H transition. However, this simulation can be considered only as a continuation of the analytic theory and, since both j_L and j_{NC} consist of the same current carriers, a self-consistent guiding-center particle simulation is required to confirm these results.

3.4 Self-consistent simulation of neoclassical radial current balance

The $E_r \times B$ flow shear has been shown to have a stabilizing effect on plasma turbulence level. This is assumed to explain the transport barriers observed at the plasma edge in many tokamaks. In a transport barrier, turbulence is strongly suppressed. The birth mechanism of the radial electric field and its shear are still not completely understand. As reviewed in Section 2.4, determining E_r from the radial current balance has been considered by many authors under various approximations and simplifications. For example, a circular geometry is often assumed. Although some of the simplifications made in the analytic expressions of the current component rising from the neoclassical bulk viscosity were tested in Section 3.2, these expressions may not be valid at the edge where the density and temperature gradients are large. Also, the effect of ion orbit losses on shear formation may suffer from the simplifications made in analytic theory. A numerical simulation of the non-ambipolar ion orbit loss current presented in the previous section is limited by some of these same assumptions, since the separation of the neoclassical return current contribution from the ion orbit loss current is not trivial.

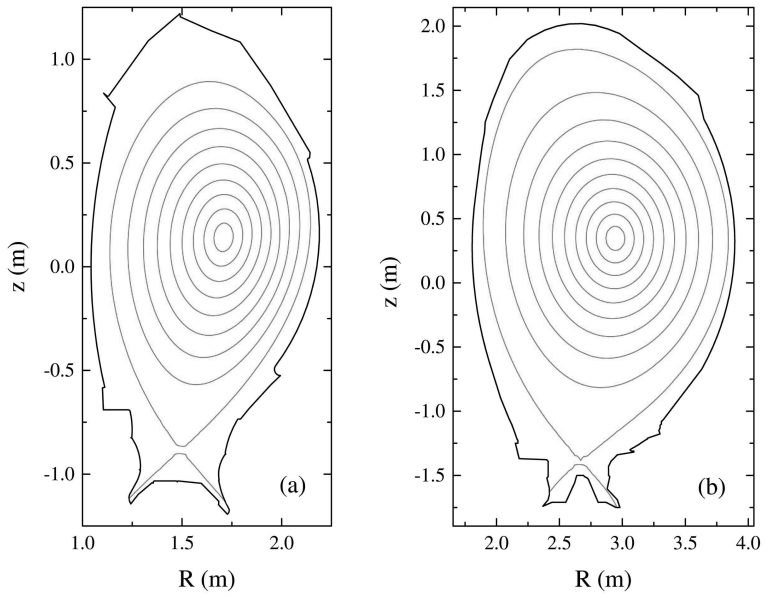

Figure 3.5: *Real magnetic field background data, including wall and divertor structures, from experimental data bases of a) ASDEX Upgrade, and b) JET is used in the simulations.*

Here, E_r is solved from the current balance, but now solving all the neoclassical current components self-consistently with the fully kinetic five-dimensional ASCOT simulation. Thus, many of the assumptions made in earlier analytic and numerical fluid models are avoided. Simulation of the tokamak plasma edge is done in realistic ASDEX Upgrade and JET divertor geometries (see Fig. 3.5). The validity of the analysis is not limited to some special collisionality regime, the thin orbit approximation is not needed, the effect of radial electric field on ion orbits is correctly modeled even for high Mach numbers, and there is no need to make various assumptions in order to separate different current components, but they are consistently evaluated from the guiding-center motion. The applied numerical model is presented in Section 3.4.1. In Section 3.4.2, the E_r profiles are simulated as a function of various parameters, and in Section 3.4.3 these profiles are compared to the critical shear for strong turbulence suppression.

3.4.1 Numerical methods

The radial electric field on a magnetic surface is solved from the radial current balance, $\langle j_r \rangle = 0$, for the radial current density j_r (quasineutrality condition). This corresponds to resolving the gyrokinetic Poisson relation in the limit of $\mathbf{k} = 0$, where $\mathbf{k}$ is the wave vector. Here, all the turbulence is neglected except for the geodesic acoustic modes [66] included in the electrostatic model. The radial current is

$$j_r(\rho, \theta) = j_{NCa} + j_{polr} + j_{visc}$$

in which j_{NCa} is the neoclassical radial ion current arising from standard guiding-center drifts in the presence of ion-ion collisions including also the effect of ion orbit losses. The polarization current, j_{polr}, is here written separately, and also the gyroviscosity current, j_{visc}, which is not a genuine guiding-center drift, is included in j_r. Current components j_{visc} and j_{polr} are generated by assigning, locally each ion the following radial drifts [67]

$$v_{visc} = -(\eta/\Omega B)[\partial^2 E_r(\rho,\theta)/\partial\rho^2]|\nabla\rho|^2, \tag{3.2}$$
$$v_{pol} = (1/\Omega B)\partial E_r(\rho,\theta)/\partial t. \tag{3.3}$$

Here, the perpendicular (gyro)viscosity coefficient is given by [68] $\eta = \eta_{Br} \equiv (3/10)k_B T\nu_{ii}/m\Omega^2$. The evolution equation for E_r derived in Section 2.4 can thus be written as

$$\frac{\partial E_r}{\partial t} = -\frac{1}{\epsilon_\perp \epsilon_0}\left\langle j_r - j_{polr}\right\rangle \approx -\frac{1}{\epsilon_\perp \epsilon_0}\left\langle j_{NCa} + j_{visc}\right\rangle, \tag{3.4}$$

where $\langle j_{NCa} + j_{visc}\rangle$ is determined from the collective motion of the test particles. A steady-state is found by extending the calculation over several bounce periods and collision times. A more detailed description of the method is given in Publication 6. Alternatively, a steady-state with $\partial E_r/\partial t = 0$ can be found by directly iterating the E_r-profile until the given n profile is established. This method is presented and derived in Publication 7. Both methods have resulted in the same steady-state, independent of the initial E_r, indicating that the final state is stable and unique.

For the radial electric field, the ambipolar $E_r(\rho)$ from Eq. (2.8) is used as the initial condition, and it is also used as an boundary condition at the inner boundary. At the separatrix, $E_r(\rho_s) = 0$ is adopted. The ions hitting the divertor or wall are promptly reinitialized at the separatrix. The reinitialization is uniform in pitch and poloidal angle, with the local Maxwellian velocity distribution. This reinitialization does not create any unphysical current in the simulation domain and, being more uniform (in phase space) than the loss process, it simulates well the replacement of charge lost through the separatrix. The binary collision model is used as a default in ASCOT, but in the present problem collisions with fixed background are used in longer runs since the aim is to obtain the result for a given temperature profile. When using the energy conserving collision operator the plasma would cool all the time since the lost particles, which are mainly energetic, are replaced by thermal particles. Thus, to maintain the experimental radial temperature, the plasma is artificially heated with the collisions with a fixed Maxwellian background.

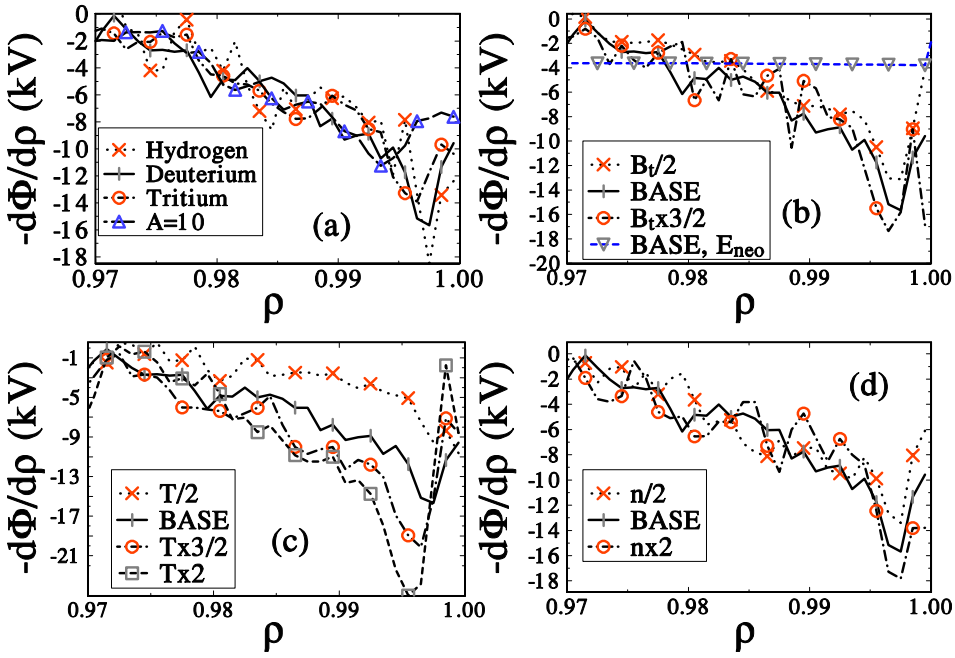

Figure 3.6: $-d\Phi/d\rho$ *as a function of radius for various plasma a) isotope, b) magnetic field, c) temperature and d) density, where 'BASE' refers to the JET L–H transition conditions. In b) also the neoclassical ambipolar level (for* $U_{\|} \approx 0$*) from analytic theory is shown for the reference case (dashed line).*

3.4.2 The dependence of the E_r profile on various plasma parameters

In Publication 5, simulated E_r profiles are shown as a function of A, B_t, T and n for the ASDEX Upgrade discharge #8044. Here, A is the mass number. In Publication 6, the same simulation is repeated for JET using data from discharge #49511 (deuterium plasma). In both cases, data at the time of the L–H transition is used. Here, the results of both simulations are summarized and the profiles for the JET case are shown. Parameters in the reference cases (referred to as 'BASE' in the figures) are given in Table 1. Here, $L_n = |n/n'|$ and $L_T = |T/T'|$ are the gradient scale lengths, and, n_s and T_s are the separatrix density and temperature (at $\rho = 1$). In the table, values on the outboard equator at the separatrix are given for the gradient scale lengths and $\nabla\rho$. In both reference cases elongation is ≈ 1.6 and the ∇B drift is in favorable direction, i.e., towards the divertor plates. Errors in the measurements of density and temperature can be tens of percents.

Table 1. Reference parameters for ASDEX Upgrade (AUG) and JET.

case	a(m)	R(m)	B_t(T)	I(MA)	L_n(m)	L_T(m)	n_s(m^{-3})	T_s(eV)	$\nabla\rho$(m^{-1})
AUG	0.5	1.65	-2.5	1	0.023	0.026	1.2e19	120	1.73
JET	≈ 1	3	-2.56	2.5	0.205	0.09	1.4e19	315	0.87

Fig. 3.6a shows the steady-state profiles of $-d\Phi/d\rho$ for JET in the region $0.97 < \rho < 1$ for plasmas consisting of various hydrogen isotopes. Also a fictive hydrogen isotope

with mass $A = 10$ is included to show the mass effect. A difference in the curves can only be seen in about a one centimeter wide region inside the separatrix. Further inside the results are almost identical. For the hydrogen ($A = 1$), one obtains a narrow and deep E_r structure which widens and becomes lower as a function of increasing mass number. As discussed in Ref. [69], the width of the E_r structure is extended to Min(r_p, L_r) from separatrix where the poloidal Larmor radius is $r_p = v_T m/eB_p$ which in this case at the outboard equator gives $r_p \approx A^{1/2}0.5$ cm. Here, $L_r = v_r/\nu_{ii}$ is the radial mean free path based on Coulomb collisions, and v_r is the radial drift velocity of the ion. Since $v_r \propto T/ZBR$ we obtain $L_r \propto T^{5/2}A^{1/2}/Z^5 nBR$ for the radial mean free path. For further inside the plasma, $|r - a| > 1 - 3$ cm, where the ion orbit losses become insignificant, E_r is at its neoclassical ambipolar level (determined by $U_\parallel = 0$ and shown in Fig. 3.6b).

In Figs. 3.6b–d, the steady-state profiles of $-d\Phi/d\rho$ are shown for deuterium plasmas for cases where the toroidal magnetic field, temperature and density profiles are changed by scaling the values of the reference case by a constant factor, respectively. As for ASDEX Upgrade, also here a clear effect is found only when changing the temperature. As shown in Fig. 3.6c, the $E\times B$ shear increases approximately linearly as a function of temperature if the gradient length is kept constant. Figs. 3.6b and d show that increasing B_t or n both slightly deepen the well just inside the separatrix, but at the inner plasma, the changes are very small. No bifurcative solutions predicted earlier in an analytic model [30], were found here. In these simulations, $L_r \gg r_p$ (except in the lowest T cases) and, thus, E_r structure is determined by r_p. At the ASDEX Upgrade case, L_r and r_p are of the same order. However, if the impurities are taken into account, L_r may dominate in both cases because L_r strongly decreases as a function of Z. Also, for helium L_r is smaller and a higher edge T is required to obtain the same shear in the $E_r \times B$ flow.

The dominant part of the shear increase is assumed to come from the ion orbit loss effect. When T increases, the orbit width grows, the mean free path of the particles increases since ν_{ii} decreases, and the radial drift velocity also increases. All these effects increase the ion orbit loss, especially just inside the separatrix. In standard neoclassical theory, the neoclassical return ion flux arising from guiding-center drifts in the presence of Coulomb collisions (but excluding ion orbit losses) is an increasing function of E_r for $M_p < 1$. This means that increasing the ion orbit loss requires higher return ion flux, i.e., higher E_r, in order to get the current balance. When going further in, the ion orbit loss flux decreases fast (dependence $\exp[-(r-a)^2/r_p^2]$ is given in Ref. [51]) and, thus, its effect on E_r decreases strongly as a function of radius causing a radial gradient in E_r. The absence of a bifurcation in the numerical simulations gives support to models [49, 51, 69], in which ion orbit loss current is assumed to have a similar dependence on E_r as the neoclassical return current, e.g., $\exp(-M_p^2)$, rather than the almost constant loss current which was assumed in Ref. [30] for $|M_p| < 1$. A strong dependence on T and a weak dependence on A, n and B_t, that were found here, have also been predicted with a semianalytical analysis in a circular geometry in Ref. [69].

In experiments, the threshold power needed for an L–H transition is essentially higher when the ∇B drift is away from the X-point (unfavorable direction) than when the drift is towards it (favorable direction). For this reason, the effect of reversing the direction of B_t keeping n and T profiles and all the other parameters unchanged was also studied in Publication 6. Within the limits of accuracy of the simulation, the E_r profiles do not change when B_t is reversed. Thus, the simulations with reversed magnetic field can not explain the difference in L–H transition power threshold unless one assumes that the critical shear is different in the reversed field case.

3.4.3 Comparison to critical shear

From Ref. [70] an expression

$$\omega_{E\times B} = \frac{(RB_p)^2}{B}\frac{\partial^2\Phi}{\partial\psi^2} = \frac{(RB_p)^2}{B}\left(\frac{\partial}{\partial\psi}\right)\frac{E_r}{RB_p} \tag{3.5}$$

for the $E \times B$ flow shearing rate is obtained. Eq. (3.5) gives significantly higher shear at the low field side of the tokamak, which is consistent with the fact that the changes taking place inside the separatrix at the L–H transition are often initiated at the outboard equator [54]. Thus, the shear values obtained from the simulation are also analyzed there. In a series of ASCOT simulations, the plasma temperature, density, and toroidal magnetic field have been varied over a wide parameter range of ASDEX Upgrade and JET data. For the parametric dependence of the E_r-shear for ASDEX Upgrade we obtain

$$\omega_{E\times B} \propto T^{1.06} n^{0.06} B_t^{-0.81}\ [s^{-1}], \tag{3.6}$$

and for JET

$$\omega_{E\times B} \propto T^{1.2} n^{0.26} B_t^{-0.89}\ [s^{-1}], \tag{3.7}$$

with a ± 0.25 error margin in the exponents. Also, I_p (or safety factor q_{95}) values have been varied, but not enough to make definitive conclusions.

In experiments, scalings for the critical temperature for an L–H transition have been obtained recently both at ASDEX Upgrade [71] and JET [72] as a function of B_t, n, and I_p or q. Comparison of these scalings shows that for typical parameters of these two tokamaks, the transition temperature is essentially higher for JET than for ASDEX Upgrade. Since the analysis of the multi-machine data base gives [73]

$$T_{e90} = 142 q_{95}^{-0.53} B_t^{0.99} R^{0.93} n_{e90}^{-0.13} \delta^{0.12} \tag{3.8}$$

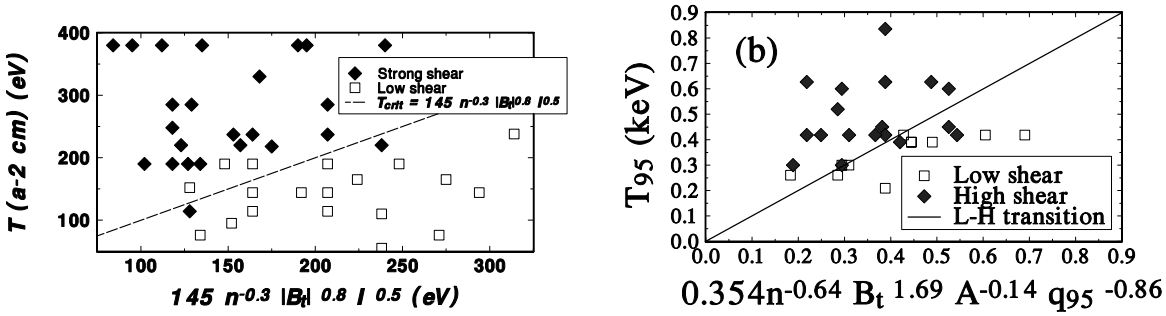

Figure 3.7: *Shear values of $E \times B$ flow from ASCOT simulation as a function of experimental parametrization of critical temperature of L–H transition for a) ASDEX Upgrade and b) JET. Experimental critical temperature is shown as a straight line in the figure.*

for the L–H transition threshold temperature, the difference between the two devices can be explained by the different major radius. Here, δ is the triangularity. The dependence on major radius may arise, for example, due to mean free path that decreases as a function of R and thus higher T is required to obtain wide enough high shear region for strong turbulence suppression. Larger major radius also decreases ion orbit loss current, which depends on the radial drift velocity $v_r \propto T/R$.

Assuming that the L–H transition occurs when a critical shear ω_{crit} is exceeded, the parametric dependence of the obtained shear values can be compared to the experimental scaling of the L–H transition threshold temperature. In Figs. 3.7a and b, the ASDEX Upgrade simulations are compared to the scaling of Ref. [71], and the shear values of JET simulations are compared to the scaling of Ref. [72]. Experimental scalings are given in horizontal labels of each figure. Here, an *ad hoc* criterion for ω_{crit} is chosen separately for ASDEX Upgrade and for JET to get the best fit between the numerical and experimental results. The chosen criterion has to be fulfilled over a turbulence decorrelation length from the separatrix, at least. In ASDEX Upgrade case the criterion $\omega_{crit} = 5 \times 10^5$ s^{-1}, and in the JET case the criterion $\omega_{crit} = 1.5 \times 10^5$ s^{-1}, gives the best fit. This can be compared to the BDT (Biglari-Diamond-Terry) criterion for the strong suppression of turbulence (see Fig. 1.2 in Introduction) which is $|\nabla E/B| > \Delta\omega_t/k_\theta \Delta r_t$ [27]. Typical values of turbulence parameters observed at DIII-D are $\Delta\omega_t = 2.5 \times 10^5$ s^{-1}, $\Delta r_t = 0.7$ cm^{-1} and $k_\theta = 1$ cm^{-1} [74], which would give a threshold shear of 3.6×10^5 s^{-1}. Similar values for ω_{crit} have also been obtained directly from E_r measurements at DIII-D and, also at TEXTOR [75]. Thus, in both cases the criterion is in rough quantitative agreement with the experimental measurements of the critical shear. The question still remains why the critical shear in the JET example seems to be lower than in the ASDEX Upgrade case. The main differences in these two examples are the values of plasma current, threshold temperature and the profile widths at the edge. The critical shear as a function of A, B_t and I_p has been studied experimentally [75] in

TEXTOR-94 and the dependence

$$\nabla E_{crit} \approx 61 \times B_t^{1.4} A^{-1.2} I_p^{-1.66} \tag{3.9}$$

in (kV m^{-2}, T, amu, MA) was found. Thus the dependence on I_p would justify using a lower threshold for JET plasmas than for the ASDEX Upgrade plasmas. In that study, the temperature dependence was not investigated. Also, if one assumes that the turbulence is due to ion temperature gradient modes, $\omega_{E\times B}$ should exceed the maximum growth rate $\gamma_{max} \sim v_T/(R^\alpha L_T^{1-\alpha})$ [54] $(0 < \alpha < 1)$ in order to stabilize the turbulence. Again, in agreement with the simulations, a lower critical shear for JET is obtained at L–H transition conditions, although the threshold temperature is higher than in ASDEX Upgrade.

It is also interesting to speculate what the threshold temperature and the critical shear would be in ITER–FEAT, which has nominal parameters $R = 6.2$ m, $I_p = 15$ MA, $B_t = 5.3$ T, and $q_{95} = 3$. Since the threshold temperature in Eq. (3.8) has the dependence $T_{thr} \propto B_t R^{0.93} q_{95}^{-0.53}$, T_{95} at L–H transition conditions would be approximately four times higher in ITER-FEAT than in JET. In the simulations, the shearing rate in Eqs. (3.6) and (3.7) has approximately the dependence $\omega_{E\times B} \approx \Upsilon(a, R, I_p, ...)T/B_t$, where $\Upsilon = \omega_{crit} B_t/T_{thr}$ can be solved using ω_{crit} obtained from the simulation and the experimental threshold temperature. From the results of this section, $\Upsilon_{JET}/\Upsilon_{AUG} \approx 0.11$ is obtained. Assuming, for example, that $\Upsilon = R^\alpha$, one obtaines $\alpha \approx -3.7$ and the critical shearing rate $\omega_{crit} \propto R^\alpha T_{thr}/B_t \propto R^{-2.76} q_{95}^{-0.53}$ would be a factor 6–7 lower for ITER-FEAT than for JET. Also, assuming that Eq. (3.9) indicates a dependence $\omega_{crit} \propto B_t^{0.4} B_p^{-1.66}$, critical shear for ITER-FEAT would be a factor of 4–5 lower than for JET.

Chapter 4

Summary and discussion

The rapid transition from low to high confinement is well documented and the important role of E_r shear in turbulence suppression is widely recognized. The radial electric field can be solved from the radial current balance, but the relative importance of different physical mechanisms affecting this balance is not fully understood. In this thesis, the electric field is evaluated from the neoclassical current balance and the parametric dependence of the shear in the electric field is investigated. Furthermore, the radial currents and parallel viscosity in a collisional regime as a response to an externally applied electric field have been explored. Most of the simulations have been done using ASDEX Upgrade parameters, but in the current balance study, JET parameters were also used for comparison. All these simulations have been performed using the 5D guiding center orbit-following Monte Carlo code ASCOT. In addition, a study of neoclassical particle fluxes in a banana regime using the 3D Fokker–Planck code DEPORA is included.

Using ASCOT, the parallel component of the momentum balance equation was investigated for several values of collisionality over a wide range of poloidal Mach numbers. It was found that, for large M_p, the parallel viscosity term changes sign in the numerical simulation. In analytic expressions, this behavior is observed only if the poloidal dependence of the density is taken into account consistently. The other components of effective viscosity, i.e., the convection and compression terms, however, are shown to dominate in a large Mach number regime. The effective viscosity has a maximum at $M_p \approx 1$, and the total effect is always to drive parallel rotation, which in turn leads to the decay of poloidal rotation. With small poloidal rotation, also the pure standard parallel viscosity term drives parallel rotation.

In the model of Ref. [30], the balance between the non-ambipolar loss of fast ions and the return current is studied and a bifurcation is found. Thus, the numerical study of both of these current components is of interest. The neoclassical ion flux in the presence of a radial electric field has been calculated in a circular geometry and compared with analytic results. The numerical result is in qualitatively agreement with the analytic result, showing a maximum at $M_p \approx 1$; quantitatively, the results

are of the same order. To isolate the influence of the various approximations and assumptions made in deriving the analytic expressions, more work is required. Based on the results the analytic expressions should be valid at least for an order of magnitude estimate of the bifurcation condition at the relevant collisionality regime. Standard neoclassical theory, however, breaks down if the density scale length is short enough, which might be the case near the edge. This effect is not investigated here.

The limitations of large aspect ratio approximation have been studied in the banana regime using DEPORA. The code solves the averaged drift-kinetic equation using the finite difference method in three dimensions. In the simulations, radial electric field was neglected, and the non-equilibrium flux due to finite density and temperature gradients was studied. When comparing the analytic and numerical results, a good agreement was found for large aspect ratios. However, as the aspect ratio decreases, the analytic expression underestimates the particle flux. Thus, the validity of large aspect ratio approximation in analytic theory is clearly limited.

As a starting point for a study of current balance in a realistic geometry, the ion orbit loss current was simulated with ASCOT as a function of collisionality and compared to the analytic expressions of the return current using ASDEX Upgrade parameters. In the model of Ref. [30], the necessary condition for a bifurcation to occur is that the non-ambipolar ion orbit loss current exceeds the maximum of the neoclassical return current, which causes the L–mode root to disappear. In separating the loss current from the bulk viscosity contribution in numerical simulation, assumptions similar to those of analytic theory were made and thus, the results similarly showed bifurcation at $\nu_* \approx 1$. Thus, the model does not explain the L–H transition, which in experiments can occur at higher collisionalities.

Since the ion orbit loss current and the neoclassical return current are carried by the same particles, separating the two is difficult in practice. Thus, it was necessary to perform a self-consistent test particle simulation of the edge plasma in which both of these effects were included in the particle motion. This simulation demonstrated that, at L–H transition conditions, pure neoclassical effects can generate sufficiently high $E \times B$ shear for strong turbulence suppression. The results additionally suggest that the critical shear in ASDEX Upgrade should be somewhat higher than in JET, which is consistent with the experimental observations and theoretical models in which critical shear decreases as a function of R, L_T or I_p. The major source for the shear originates from the ion orbit loss current, which is a strong function of both the plasma temperature and the distance from the separatrix. The width of the highest shear region in the simulation appears to approximate to the poloidal Larmor radius, in agreement with certain experimental results. Also further in, the shear can exceed the threshold shear.

Although the present simulations were able to find a cause for the high shear leading to strong turbulence suppression at L–H transition conditions, several properties of the L–H transition are not explained by the present model. The fast time scale

of the transition observed in certain experiments, for example, is not explained by the simulations, since E_r in the model follows the changes in local density and temperature that take place on a collisional time scale. No bifurcative solutions predicted earlier in analytic theory [30] were found here. Thus, the simulations agree only with those experimental results which suggest that the transition is a continuous process [76]. If a bifurcative process is needed to explain the experiments, it is likely to derive from turbulence theory rather than from neoclassical current balance. Moreover, the simulation results do not explain the hysteresis and the effect of the direction of the ∇B drift on the power threshold, which are both observed in experiments. In the simulations, the E_r profile does not change when B_t is reversed if all the other parameters are maintained fixed and, in experiments, the density and temperature profiles are similar for both directions of B_t for a given heating power. Thus, the present simulations do not explain the difference in L–H transition power threshold unless one assumes that the critical shear is different for reversed B_t.

The present fully kinetic 5D simulation does not suffer from many of the limitations of the earlier approaches, but some important simplifications should be mentioned. First, the scrape-off layer plasma was not simulated and, thus, the replacement of the lost ions by such true sources as gas puffing and recycling was not modeled from the first principles. Secondly, the boundary condition for E_r at the separatrix was arbitrarily set. However, it is shown in Publication 6 that the E_r profile inside the separatrix is affected by the boundary value only on a thin layer that is not significant when the suppression of turbulence is considered. Numerical tests also indicate that the shear in E_r inside the separatrix to a large extent can be evaluated without extending the calculation of the source of return current to the scrape-off layer. However, the poloidal distribution of this source has been found to affect the results. Thus, in the future, the experimental neutral distribution around the separatrix should be taken into account. Poloidal dependence of the plasma density and temperature profiles outside the separatrix may exert an effect on the ion orbit loss rate, but this has not been investigated here.

Although the anomalous current can often be assumed ambipolar, the anomalous convection may exert a non-ambipolar secondary effect; it may affect the loss cone population, and thus influence the non-ambipolar ion orbit loss current. Neglecting this may be a significant simplification in the current model, but inclusion of the effect is far beyond the scope of this thesis. However, there are plans to incorporate anomalous transport effects in the simulation by developing a gyrokinetic version of the ASCOT code. With a gyrokinetic ASCOT, simulation of turbulence in a realistic tokamak geometry becomes possible. For example, turbulence-driven small scale zonal flows, which can reduce the thermal diffusivity [77], can be simulated without many of the approximations made in earlier approaches. Furthermore, resistive X-point modes [78], which may be dominant contributors to turbulent diffusion in the boundary plasma of a diverted tokamak, can be simulated without the limitations associated with the Braginskii fluid model.

Bibliography

[1] M. Keilhacker *et al*, "High fusion performance from deuterium-tritium plasmas in JET", Nucl. Fusion **39**, 209 (1999).

[2] M.N. Rosenbluth, "Physics fundamentals for ITER", Plasma Physics and Controlled Fusion **41**, A99 (1999).

[3] Adopted from M.J. Mantsinen, "Development and experimental evaluation of theoretical models for ion cyclotron resonance frequency heating of tokamak plasmas", Report TKK-F-A789, Helsinki University of Technology, Espoo, 1999.

[4] F.L. Hinton and R.D. Hazeltine, "Theory of plasma transport in toroidal confinement systems", Rev. Mod. Phys. **48**, 239 (1976).

[5] R.E. Potok, P.A. Politzer, and L.M. Lidsky, "Ion thermal conductivity in a helical toroid", Phys. Rev. Lett. **45**, 1328 (1980).

[6] R.H. Fowler, J.A. Rome, and J.F. Lyon, "Monte Carlo studies of transport in stellarators" Phys. Fluids **28**, 338 (1985).

[7] H.E. Mynick, "Verification of the classical theory of helical transport in stellarators", Phys. Fluids **25**, 325 (1982).

[8] W. Lotz and I. Nürenberg, "Monte Carlo computations of neoclassical transport", Phys. Fluids **31**, 2984 (1988).

[9] C.D. Beidler, W.N.G. Hitchon, D.L. Grekov, and A.A. Shishkin, "Monte Carlo evaluation of neoclassical transport in torsatrons with different helical winding laws", Nucl. Fusion **30**, 405 (1990).

[10] A.H. Boozer, G. Kuo-Petravic, "Monte Carlo evaluation of transport coefficients", Phys. Fluids **24**, 851 (1981).

[11] M. Taguchi, "A method for calculating neoclassical transport coefficients with momentum conserving collision operator", Phys. Fluids B **4**, 3638 (1992).

[12] S.P. Hirshman, P.D. Sigmar, "Neoclassical transport of impurities in tokamak plasmas", Nucl. Fusion **21**, 1079 (1981).

[13] A.L. Rogister, "Revised neoclassical transport theory for steep, collisional plasma edge profiles", Phys. Plasmas **1**, 619 (1994).

[14] P. Helander, "Bifurcated neoclassical particle transport", Phys. Plasmas **5**, 3999 (1998).

[15] A.L. Rogister, "Transport barriers formation and subneoclassical energy fluxes: a unified theoretical approach", Phys. Rev. Lett. **81**, 3663 (1998).

[16] K.C. Shaing, "Poloidal and parallel plasma viscosities in tokamak geometry", Phys. Fluids B **2**, 2847 (1990).

[17] K. C. Shaing and C. T. Hsu, "Convective momentum transport, shock viscosity, and the L-H transition in tokamaks", Phys. Fluids B **5**, 2981 (1993).

[18] M. Endler *et al*, "Measurements and modelling of electrostatic fluctuations in the scrape-off layer of ASDEX" Nucl. Fusion **35**, 1307 (1995).

[19] ITER Confinement Database and Modelling Working Group, "Energy confinement scaling and the extrapolation to ITER", Plasma Phys. Control. Fus. **39**, B115 (1997).

[20] X. Garbet, "Towards a full self-consistent numerical simulation of tokamak plasma turbulence", Plasma Phys. Control. Fus. **39**, B91 (1997).

[21] R.D. Stambaugh *et al*, "Enhanced confinement in tokamaks", Phys. Fluids B **2**, 2941 (1990).

[22] G.L. Jackson *et al*, "Regime of very high confinement in the boronized DIII-D tokamak", Phys. Rev. Lett. **67**, 3098 (1991).

[23] K.H. Burrell, "Effects of $E \times B$ velocity shear on turbulence and transport in magnetic confinement devices", Phys. Plasmas **4**, 1499 (1997).

[24] F. Wagner *et al*, "Regime of improved confinement and high beta in neutral-beam-heated divertor discharges of the ASDEX tokamak", Phys. Rev. Lett. **49**, 1408 (1982).

[25] B. Lehnert, "Short-circuit of flute disturbances at a plasma boundary", Phys. Fluids **9**, 1367 (1966).

[26] P. W. Terry, "Suppression of turbulence and transport by sheared flow", Reviews of Modern Physics, **72**, 109 (2000).

[27] H. Biglari, P.H. Diamond, P.W. Terry, "Influence of sheared poloidal rotation on edge turbulence", Phys. Fluids B **2**, 1 (1990).

[28] A.B. Hassam, T.M. Antonsen, Jr., J.F. Drake, and C.S. Liu, "Spontaneous poloidal spin-up of tokamaks and the transition to H mode", Phys. Rev. Lett. **66**, 309 (1991).

[29] P.H. Diamond, Y.-B. Kim, "Theory of mean poloidal flow generation by turbulence", Phys. Fluids B **3**, 1626 (1991).

[30] K.C. Shaing and E.C. Crume, Jr., "Bifurcation theory of poloidal rotation in tokamaks: a model for the L-H transition", Phys. Rev. Lett. **63**, 2369 (1989).

[31] G.M. Staebler, R.R. Dominguez, "Turbulent viscosity bifurcation and the H-mode", Nucl. Fusion **33**, 77 (1993).

[32] J.A. Rome and Y-K.M. Peng, "The topology of tokamak orbits", Nucl. Fusion **19**, 1193 (1979).

[33] P.H. Rutherford, "Collisional diffusion in an axisymmetric torus", Physics of Fluids **13**, 482 (1970).

[34] T.E. Stringer, "Non-ambipolar neoclassical transport", Nucl. Fusion **35**, 1008 (1995).

[35] V. Rozhansky *et al*, in Controlled Fusion and Plasma Physics (Proc. 18th Eur. Conf. Berlin, 1991) Vol. 15C, Part IV, European Physical Society, Geneva, 287 (1991).

[36] T.H. Stix, "Decay of poloidal rotation in a tokamak plasma", Phys. Fluids **16**, 1260 (1973).

[37] S.P. Hirshman, "The ambipolarity paradox in toroidal diffusion, revisited", Nucl. Fusion **18**, 917 (1978).

[38] T.E. Stringer, "Equilibrium diffusion rate in a toroidal plasma at intermediate collision frequencies", Phys. Fluids **13**, 810 (1970).

[39] J. Cornelis *et al*, "Predicting the radial electric field imposed by externally driven radial currents in tokamaks", Nucl. Fusion **34**, 171 (1994).

[40] L.M. Kovrizhnykh, "Neoclassical theory of transport processes in toroidal magnetic confinement systems, with emphasis on non-axisymmetric configurations", Nuclear Fusion **24**, 851 (1984).

[41] K.C. Shaing *et al*, "Bifurcation and relaxation of radial electric field in enhanced reversed shear tokamak plasmas", Phys.Rev.Lett. **83**, 3840 (1999).

[42] O. Dumbrajs *et al* (among them T.P. Kiviniemi), "Triggering Mechanisms for Transport Barriers", 18th International Conference on Fusion Energy, Sorrento, Italia, October 4-10, 2000, Paper, 6 pp.

[43] T.E. Stringer and J.W. Connor, "Generalized equations for plasma of arbitrary collision frequency in weakly inhomogeneous magnetic field", Phys. Fluids **14**, 2177 (1971).

[44] E.P. Gross, M.Krook, Phys. Rev. **102**, 593 (1956).

[45] J.W. Connor and T.E. Stringer, "Diffusion of an equilibrium toroidal plasma at intermediate and higher collision frequencies", Phys. Fluids **14**, 2184 (1971).

[46] K.C. Shaing, R.D. Hazeltine, H. Sanuki, "Shock formation in a poloidally rotating tokamak plasma", Phys. Fluids B **4**, 404 (1992).

[47] K.C. Shaing, E.C. Crume Jr., W.A. Houlberg, "Bifurcation of poloidal rotation and suppression of turbulent fluctuations: A model for the L-H transition in tokamaks", Phys. Fluids B **2**, 1492 (1990).

[48] K. Itoh and S-I. Itoh, "Review article: The role of the electric field in confinement", Plasma Phys. Control. Fusion **38**, 1 (1996).

[49] S.-I. Itoh, K. Itoh, "Model of the H-mode in tokamaks", Nucl. Fusion **29**, 1031 (1989).

[50] K.C. Shaing and P.J. Christenson, "Ion collisionality and L-H transition in tokamaks", Phys. Fluids B **5**, 666 (1993).

[51] A. Fukuyama, Y. Fuji, K. Itoh, and S.-I. Itoh, "Transport modelling including electric field and plasma rotation", Plasma Phys. Control. Fusion **36**, A159 (1994).

[52] A. Fukuyama, Y. Fuji, S.-I. Itoh, M. Yagi, and K. Itoh, "Transport modelling of L-H transition and barrier formation", Plasma Phys. Control. Fusion **38**, 1319 (1996).

[53] J.A. Heikkinen *et al* (among them T.P. Kiviniemi), "Bifurcation and the radial electric field in the presence of edge polarization in tokamaks", Phys. Plasmas **8**, 2824 (2001).

[54] J.W. Connor, and H.R. Wilson, "A review of theories of the L-H transition", Plasma Phys. Control. Fusion **42**, R1 (2000).

[55] M. Tendler, "Different scenarios of transitions into improved confinement modes", Plasma Phys. Control. Fusion **39**, B371 (1997).

[56] Z.S. Zaitsev, M.R. O'Brien, M. Cox, "Three-dimensional neoclassical nonlinear kinetic equation for low collisionality axisymmetric tokamak plasmas", Phys. Fluids B **5**, 509 (1993).

[57] S. Ma, R.D. Sydora, J.M. Dawson, "Binary collision model in gyrokinetic simulation plasmas", Comput. Phys. Commun. **77**, 190 (1993).

[58] T.P. Kiviniemi, "Neoclassical fluxes in a tokamak and the role of ion orbit loss in the L–H transition", Report TKK-F-B177, Helsinki University of Technology, Espoo, 1998.

[59] S. Sipilä, "Monte Carlo simulation of charged particle orbits in the presence of radiofrequency waves in tokamak plasmas", dissertation, Helsinki University of Technology, Espoo (1997), ISBN 951-22-3856-X.

[60] J.A. Heikkinen, S.K.Sipilä, "Power transfer and current generation of fast ions with large-k_θ waves in tokamak plasmas", Phys. Plasmas **2**, 3724 (1995).

[61] J.A. Heikkinen, S. Sipilä, and T.J.H. Pättikangas, "Monte Carlo simulation of runaway electrons in a toroidal geometry", Comput. Phys. Commun. **76**, 215 (1993).

[62] S. Sipilä and J.A. Heikkinen, "Monte Carlo simulation of lower hybrid current drive in tokamaks", IEEE Transactions on Plasma Science **22**, 260 (1994).

[63] R.B. White and A.H. Boozer, "Rapid guiding center calculations", Phys. Plasmas **2**, 2915 (1995).

[64] T.S. Taylor, "Physics of advanced tokamaks", Plasma Phys. Contr. Fusion **39**, B47 (1997).

[65] T.E. Stringer, "Neoclassical transport in the presence of fluctuations", Nucl. Fusion **32**, 1421 (1992).

[66] S.V. Novakovskii, C.S. Liu, R. Sagdeev, and M.N. Rosenbluth, "The radial electric field dynamics in the neoclassical plasmas", Phys. Plasmas **4**, 4272 (1997).

[67] L. Spitzer, "Physics of Fully Ionized Gases", 2nd Ed., Interscience Publishers, 1962, New York; Eq. 2.42.

[68] S.I. Braginskii, Reviews of Plasma Physics (Consultants Bureau, New York, 1965) Vol.1.

[69] J.A. Heikkinen, T.P. Kiviniemi, and A.G. Peeters, "L-H Transport Barrier Formation: Monte Carlo Simulation of the Sheared ExB - Flow Dynamics in Tokamaks", Contrib. Plasma Phys. **40**, 431 (2000).

[70] T.S. Hahm and K.H. Burrell, "Flow shear induced fluctuation suppression in finite aspect ratio shaped tokamak plasma", Phys. Plasmas **2**, 1648 (1995).

[71] W. Suttrop *et al*, "Identification of plasma-edge-related operational regime boundaries and the effect of edge instability on confinement in ASDEX Upgrade", Plasma Phys. Contr. Fusion **39**, 2051 (1997).

[72] E. Righi *et al*, "Comparison between experimental and theoretical conditions for the L–H transition in JET", Plasma Phys. Control. Fusion **42**, A199 (2000).

[73] J.A. Snipes and the International H–mode Threshold Database Working Group, "Latest results on the H–mode threshold using the international H–mode threshold database", Plasma Phys. Control. Fusion **42**, A299 (2000).

[74] P. Gohil, K.H. Burrell, and T.N. Carlstrom, "Parametric dependence of the edge radial electric field in the DIII-D tokamak", Nucl. Fusion **38**, 93 (1998).

[75] S. Jachmich and R. R. Weynants, "Efficiency of transport suppression due to ExB flow shear - a parameter study", Plasma Phys. Control. Fusion **42**, A147 (2000).

[76] J. Hugill, "Edge turbulence in tokamaks and the L–mode to H–mode transition", Plasma Phys. Control. Fus. **42**, R75 (2000).

[77] Z.Lin *et al*, "Effects of collisional zonal flow damping on turbulent transport", Phys. Rev. Lett. **83**, 3645 (1999).

[78] J.R. Myra *et al*, "Resistive X-point modes in tokamak boundary plasmas", Phys. Plasmas **7**, 2290 (2000).